Extracellular vesicles released by polycyclic aromatic hydrocarbons-treated hepatocytes trigger oxidative stress in recipient hepatocytes by delivering iron

Nettie van Meteren[a], Dominique Lagadic-Gossmann[a], Normand Podechard[a], Dimitri Gobart[a], Isabelle Gallais[a] Martine Chevanne[a], Aurore Collin[a,1], Agnès Burel[b], Aurélien Dupont[b], Ludivine Rault[d], Soizic Chevance[c], Fabienne Gauffre[c], Eric Le Ferrec[a], Odile Sergent[a].

[a] *Univ Rennes, Inserm, EHESP, Irset (Institut de recherche en santé, environnement et travail) - UMR_S 1085, F-35000 Rennes, France*

[b] *Univ Rennes, Biosit – UMS 3480, US_S 018, F-35000 Rennes, France*

[c] *Univ Rennes, CNRS, ISCR (Institut des sciences chimiques de Rennes) – UMR 6226, F-35000 Rennes, France*

[d] *Univ Rennes, ScanMAT – UMS 2001, F-35000-Rennes, France*

[1] *Present address : Université Clermont-Auvergne, NEURO-DOL, Inserm U1107, 2, rue Braga, 63100 Clermont-Ferrand, France.*

Corresponding author : Odile Sergent ; IRSET, Faculté de Pharmacie ; 2, av Pr. Léon Bernard; 35043 Rennes Cedex ; France

E- mail address : odile.sergent@univ-rennes1.fr

Telephone : 33(0)223234808 Fax : 33(0)223235055

ABSTRACT

A growing body of evidences indicate the major role of extracellular vesicles (EVs) as players of cell communication in the pathogenesis of liver diseases. EVs are membrane-enclosed vesicles released by cells into the extracellular environment. Oxidative stress is also a key component of liver disease pathogenesis, but no role for hepatocyte-derived EVs has yet been described in the development of this process. Recently, some polycyclic aromatic hydrocarbons (PAHs), widespread environmental contaminants, were demonstrated to induce EV release from hepatocytes. They are also well-known to trigger oxidative stress leading to cell death. Therefore, the aim of this work was to investigate the involvement of EVs derived from PAHs-treated hepatocytes (PAH-EVs) in possible oxidative damages of healthy recipient hepatocytes, using both WIF-B9 and primary rat hepatocytes. We first showed that the release of EVs from PAHs -treated hepatocytes depended on oxidative stress. PAH-EVs were enriched in proteins related to oxidative stress such as NADPH oxidase and ferritin. They were also demonstrated to contain more iron. PAH-EVs could then induce oxidative stress in recipient hepatocytes, thereby leading to apoptosis. Mitochondria and lysosomes of recipient hepatocytes exhibited significant structural alterations. All those damages were dependent on internalization of EVs that reached lysosomes with their cargoes. Lysosomes thus appeared as critical organelles for EVs to induce apoptosis. In addition, pro-oxidant components of PAH-EVs, e.g. NADPH oxidase and iron, were revealed to be necessary for this cell death.

Key words : Polycyclic aromatic hydrocarbons, extracellular vesicles, hepatocytes, NADPH oxidase, ferritin, LMW iron, lipid peroxidation, lysosomes, mitochondria

Abbreviations : AhR , aryl hydrocarbon receptor; APO, apocynin; BAF, bafilomycin A1; BP, benzo(a)pyrene; CyB, cytochalasin B; CYP1, cytochrome P450 family 1; DBA, dibenzo(a,h)anthracene; DFO, desferrioxamine; DFP, deferiprone; EDS, energy dispersive X-ray

spectroscopy; EROD, ethoxyresorufin-O-deethylase; EV, extracellular vesicle; FTL, ferritin light chain; LMW iron, low-molecular-weight iron; MCD, methyl-β-cyclodextrin; NTA, nanoparticle tracking analysis; PAH, polycyclic aromatic hydrocarbon; PAH-EVs, EVs derived from PAH-treated hepatocytes; PYR, pyrene; ROS, reactive oxygen species; Th, thiourea; VitE, vitamin E; Wort, wortmannin.

1. INTRODUCTION

Extracellular vesicles (EVs), *i.e.* membrane-enclosed vesicles released by cells into the extracellular environment, are now recognized as important mediators of intercellular communication [1]. Depending on the initial stimulus of their production, EVs are specifically enriched in cargoes such as proteins, lipids, and nucleic acids that can be transferred into recipient cells [2,3], thereby modulating cell functions. As liver is a multicellular organ composed of hepatocytes and non-parenchymal cells, a role for EVs has emerged in the pathogenesis of liver diseases, such as hepatitis, cirrhosis and hepatocellular carcinoma [4–6]. Thus, hepatocyte-derived EVs have been described to activate [7] or recruit [8,9] macrophages, to activate stellate cells [10,11] and endothelial cells [12,13], thus leading to inflammation, fibrogenesis and angiogenesis, processes well-known to participate in the development of liver diseases.

Whereas oxidative stress is considered as a key event in the pathogenesis of liver diseases [14–16], nothing is known about its possible induction in cells targeted by hepatocyte-derived EVs. However, EVs isolated from some extrahepatic tissues have been reported to generate reactive oxygen species (ROS) in recipient cells. Thus, the large EVs, *i.e.* microvesicles, essentially isolated from circulating cells or from endothelial cells, have been recently reviewed as ROS producers in recipient cells [17]. Besides, exosomes, the smaller type of EVs, when released from skin keratinocytes [18], melanoma cell lines [19] or breast cancer cells [20], were able to cause an increase in ROS levels in recipient cells. However, in all cases, no proof of an oxidative damage was provided. Regarding cells producing EVs, a role for oxidative stress in the EV release by pulmonary fibroblasts [21] or bronchial epithelial cells [21,22] has already been shown, but nothing is known yet concerning hepatocytes.

Recently, for the first time in the field of toxicant-associated liver diseases, some polycyclic aromatic hydrocarbons, widespread environmental contaminants, were demonstrated to stimulate hepatocytes to release EVs with a modified composition and

structure, as a mirror of mechanisms involved in PAH-induced cell death [23]. Interestingly, PAHs have also been described to induce cell death by mechanisms that implicated oxidative stress. For instance, benzo(a)pyrene (BP) can promote ROS production in liver cells both *in vitro* [24,25] and *in vivo* [26], leading to oxidative damages such as lipid peroxidation in cultured liver cells [27,28] or in mice liver [29], as well as DNA oxidation in hepatocytes [30] or in rat liver [31]. Those oxidative damages were demonstrated to be responsible for cell death in liver [27,28,32,33]. Pyrene (PYR) can also trigger ROS production in hepatocytes along with a decrease in the expression of antioxidant enzymes, thus leading to a loss of viability [34]. In mice, the depletion in the antioxidant glutathione was associated to PYR-induced liver damage [35].

Although oxidative stress is a key component of the pathogenesis of liver diseases, no role for hepatocyte-derived EVs has yet been described in the development of this process. Therefore, we decided to investigate the involvement of EVs derived from hepatocytes treated by PAHs in possible oxidative effects in healthy recipient hepatocytes. Particular attention was also paid to the role of oxidative stress for their release. Using hepatocytes from both WIF-B9 cell line and primary rat cultures, we demonstrated that EVs derived from PAH-treated hepatocytes were able to induce oxidative stress in recipient hepatocytes notably *via* an iron enrichment of those EVs.

2. MATERIALS AND METHODS

2.1. Chemicals

Benzo(a)pyrene (BP), dibenzo(a,h)anthracene (DBA), pyrene (PYR), N-acetyl-Asp-Glu-Val-Asp-7-amido-4 methylcoumarin (Ac-DEVD AMC), Hoechst 33342, dimethyl sulfoxide (DMSO), cytochalasin B (CyB), methyl-β-cyclodextrin (MCD), wortmannin (Wort), bafilomycin A1 (BAF), desferrioxamine (DFO), thiourea (Th) and vitamin E (VitE) were all purchased from Sigma–Aldrich (Saint Quentin Fallavier, France). SYTOX®Green was

obtained from Life Technologies (Thermo Fisher Scientific Courtaboeuf, France) and deferiprone (DFP) from Acros (Thermo Fisher Scientific Courtaboeuf, France). Dihydroethidium (DHE), C11-BODIPY$^{581/591}$, LysoTracker Red DND-99 and LysoSensor Yellow/Blue DND-160, MitoTracker red FM were obtained from Molecular Probes (ThermoFisher Scientific, Courtaboeuf, France). Apocynin was acquired from Calbiochem (Millipore, Saint-Quentin Les Yvelines, France). Mito-FerroGreen was obtained from Dojindo (Munich, Europe).

Goat polyclonal anti-FTL (ferritin light chain) antibody was purchased from Origene (Herford, Germany). Mouse monoclonal anti-HSC70, anti-gp91-phox and anti-p47-phox antibodies were acquired from Santa Cruz Biotechnology (Heidelberg, Germany). Rabbit monoclonal anti-ferritin heavy chain was purchased from Abcam (Paris, France). Horseradish peroxidase (HRP)-conjugated secondary antibodies were from Dako **(**Agilent Technologies, Courtaboeuf, France).

2.2. Cell isolation and culture

Two types of hepatocytes, primary rat hepatocytes and hybrid human/rat hepatocytes of the WIF-B9 cell line, were studied. Primary hepatocytes were used as they are physiologically and metabolically close to *in vivo* models. For longer incubation times, not suited for primary hepatocyte survival, the WIF-B9 cell line was also tested due to its high level of differentiation into hepatocytes, making it very sensitive to chemical toxicants, even at very low doses [36,37].

Primary rat hepatocytes. Adult hepatocytes were isolated from two-month-old male Sgrague Dawley rats (Janvier labs, Le Genest-Saint-Isle, France) by perfusion of the liver with a 17 µg/ml liberase (Roche Diagnostic, Meylan, France) solution to obtain liver dissociation. All protocols (project APAFIS 6675-2016) were approved by our local ethic committee CREEA (Comité Rennais d'Ethique en matière d'Expérimentation Animale), and were in agreement with the European Union regulations concerning the use and protection of experimental animals (Directive

2010/63/EU). Viability of the freshly isolated hepatocytes was routinely above 85%. Cells were seeded at densities of 1.5 x 10^6 cells in 35-mm petri dishes (Hoechst 33342 staining), 3 x 10^6 cells in 60-mm petri dishes (caspase-3/7 activity, EV isolation for NTA), 8 x 10^6 cells in 100-mm petri dishes (membrane fluidity determination and cholesterol measurement), and 15 x 10^6 cells in 150-mm petri dishes (EV isolation for protein, lipid, and EPR analysis). They were then cultured in a medium composed of 75% minimum Eagle's medium and 25% medium 199 with Hanks salts (Sigma-Aldrich, Saint-Quentin-Fallavier, France), supplemented with 10% fetal calf serum (FCS) (Gibco, Illkirch, France) and containing 2.2 g/L $NaHCO_3$ and 5 µg streptomycin, 5 UI penicillin (Gibco, Illkirch, France), 3.2 µg bovine serum albumin (BSA) (Eurobio, Courtaboeuf, France), and 5 µg bovine insulin (Sigma-Aldrich, Saint-Quentin-Fallavier, France) per milliliter. Cells were incubated at 37°C under an atmosphere of 5% CO_2 and 95% air. The medium was changed 3 h following seeding and replaced by the same medium without FCS.

WIF-B9 cell line. WIF-B9 hybrid cells, obtained by fusion of Fao rat hepatoma cells and WI-38 human fibroblasts, were a generous gift from Doris Cassio (UMR Inserm S757, Université Paris-Sud, Orsay, France). WIF-B9 cells were grown in F12 Ham Coon's nutrient medium (Sigma-Aldrich, Saint-Quentin-Fallavier, France) supplemented with 5% FCS (Gibco, Illkirch, France) and containing 2.2 g/L $NaHCO_3$, 100 UI penicillin, 10 µg streptomycin, and 0.25 µg amphotericin B (Sigma-Aldrich, Saint-Quentin-Fallavier, France) per milliliter, 2 mM glutamine (Gibco, Illkirch, France), and HAT supplement [sodium hypoxanthine (10 µM), aminopterin (40 nM), and thymidine (1.6 µM)] (Gibco, Illkirch, France). Cells were incubated at 37°C in an atmosphere of 5% CO_2 and 95% air. Cells were seeded at 12.5 x 10^3 cells/cm^2 and cultured for seven days, until reaching approximately 80% of confluence, before PAH treatment. Before treatment, the medium was changed and replaced

by the same medium but previously deprived of EVs. EV depletion was obtained by ultracentrifugation of the medium containing 25% FCS, at 100,000 x g for 14 h at 4 °C.

2.3. Cell treatment

For this study, we selected the same PAHs as for our previous work [23] *i.e.* BP, DBA, and PYR based on their variable presence in food [38] and affinity for the aryl hydrocarbon receptor (AhR) [39]. In order to isolate EVs from PAH-treated hepatocytes, cells were exposed to 100 nM of each PAH, or 0.0005 % dimethyl sulfoxide (DMSO) as control cultures, for 18 h for primary rat hepatocytes and 72 h for WIF-B9 hepatocytes. This PAH concentration was chosen based on results previously published [23]. Then, to test the impact of those EVs on healthy recipient hepatocytes, a preliminary study of dose and time response on cell death was conducted in both cell types. For this purpose, they were exposed to EVs at various concentrations (2.5, 5 or 15 µg of EV proteins/mL) for various incubation times (5, 24, 48 or 72 hours for WIF-B9, and 5 or 18 hours for primary rat hepatocytes). Those EV concentrations roughly corresponded to that found in culture media of WIF-B9 hepatocytes treated for 72 hours by PAHs or of primary rat hepatocytes exposed during 18 hours. As the levels of apoptosis induced by EVs derived from PAH-treated WIF-B9 and primary rat hepatocytes were the highest at 24 hours and 18 hours, respectively (Supplementary Figure S1), the following experiments were performed using those exposure times. Concerning EV concentration, a highest apoptosis was obtained with the 5 and 15 µg/mL concentrations leading us to keep the 5 µg/mL concentration for the following experiments. In the experiments aimed at investigating the mechanisms underlying the effect of EVs on recipient hepatocytes, cultures were pre-treated with various compounds (Supplementary Table S1) for 30 min prior to co-exposure with the toxicants.

2.4. EV analysis

EV isolation from PAH-treated hepatocytes. After each treatment with toxicant, culture media were collected to isolate total EVs. The media were first centrifuged at 3,650 x g for 10 min to remove any cells, cell debris and apoptotic bodies. Total EVs were then pelleted by ultracentrifugation (Optima L-90 K Ultracentrifuge, Beckman Coulter, Villepinte, France) of the cleared supernatants at 100,000 x g for 1 h 45 min at 4°C in a SW28-1 swinging-bucket rotor (Beckman Coulter, Villepinte, France). Pellets were then washed with PBS and re-centrifuged at the same speed. Finally, EVs were re-suspended in 100 to 200 µL PBS, depending on the quantity.

Protein concentration. The protein concentrations of cell lysates and EVs were determined by the Pierce BCA protein assay kit (Thermo Fisher Scientific, Illkirch, France) using BSA as the standard. Hepatocytes were lysed in RIPA buffer (50 mM Tris buffer, 150 mM NaCl, 0.1 % SDS, 1 % Triton X-100, 0.5 % sodium deoxycholate, 50 mM NaF, 5 mM EDTA pH 8) supplemented with protease inhibitors (1 mM orthovanadate, 1 mM phenylmethylsulfonyl fluoride, 5 µg/ml leupeptin, 0.1 µg/ml aprotinin and 0.5 mM dithiothreitol) before sonication on ice.

Protein expression. Equal amounts of protein (at least 10 µg) were denatured for 5 min at 95 °C in RIPA buffer and then separated by sodium dodecyl sulfate (SDS) polyacrylamide gel electrophoresis (SDS–PAGE) using 12% or 15% polyacrylamide gels. After overnight transfer onto nitrocellulose membranes (Millipore, St Quentin-en-Yvelines, France) and blocking for 1 hour at room temperature with a TBS solution containing 5% BSA, primary antibodies were added and the membranes incubated for 2 hours at room temperature [anti-gp91-phox (1:100), anti-p47-phox (1:1000), anti-FTL (1:1000), and anti-HSC70 (1:10000)]. Then, membranes were washed three times with 0.1% Tween 20 in TBS for 10 min and incubated in blocking buffer containing appropriate horseradish peroxidase-conjugated secondary antibodies (1:2500) for 1 hour at room temperature. Following incubation, they were

washed six times with 0.1% Tween 20 in TBS for 5 min. Immunolabeled proteins were then visualized by chemiluminescence using an enhanced chemiluminescence (ECL) solution (Tris-HCl 0.1 M pH 8.5, 0.22 mM coumaric acid, 1.25 mM luminol, and 0.009 % H_2O_2) and a ChemiDoc™ XRS+analyzer, and the images processed using Image Lab 6.0 (Bio-Rad, Marnes-la-Coquette, France). HSC70 primary antibodies were used to evaluate protein loading.

Independent experiments could not be run on the same gel. Thus, the relative density ratio was calculated. First, band densities of the protein of interest (FTL, gp91-phox, p47-phox) and that of the loading controls (Hsc70) were measured on every blot and the backgrounds subtracted. Then, the density of the protein of interest in each lane was divided by the respective density of the loading control on every blot. Finally, each normalized density of the protein of interest for the EVs was divided by the normalized density of the control EVs (first lane on the blots). Each value for the control EV from independent blots was set to one, as the density ratios were systematically relative to the control EV ratio. Differences in the means of relative density ratios allowed us to compare expression levels of the proteins of interest from different blots. For multiple bands, the densities of each band were added and the sum used as the density of the protein of interest.

Cryo-electron microscopy. Vitrification of EVs was performed using an automatic plunge freezer (EM GP, Leica) under controlled humidity and temperature [40]. The samples (i.e. 10 µL of EVs at a concentration of 10^{12} particles/mL) were deposited on glow-discharged electron microscope grids followed by blotting and vitrification by rapid freezing into liquid ethane. Grids were transferred to a single-axis cryo-holder (model 626, Gatan) and were observed using a 200 kV electron microscope (Tecnai G2 T20 Sphera, FEI) equipped with a 4k × 4k CCD camera (model USC 4000, Gatan). Micrographs were acquired under low electron doses using the camera in binning mode 1 and at a nominal magnification of 25,000 X.

Iron measurement. Five microliters of the EV suspension were incubated for 20 min on formvar carbon-coated grids (Nickel Grid 300 mesh, Agar Scientific, Oxford Instruments, Gometz-la-Ville, France). Excess liquid was removed by blotting and the grid was then negatively stained with 2% uranyl acetate followed by blotting to remove excess liquid. Samples were imaged using a Jeol JEM 2100 HR microscope (JEOL Ltd, JEOL Europe SAS, Croissy-sur-Seine, France) operated at an acceleration voltage of 200 kV, equipped with a Gatan Orius SC200D camera (Gatan Inc) and coupled with an Energy Dispersive X-Ray Spectroscopy (EDS) analyser EDX Oxford X-Max 80T that characterizes the elemental composition.

EV uptake by recipient cells. EVs were first labelled using the PKH67 Green Fluorescent Cell Linker Kit (Sigma–Aldrich, Saint Quentin Fallavier, France). Briefly, following the manufacturer's instructions, the washed EV pellets were resuspended in 250 µL of Diluent C and then mixed with 250 µL of a solution of 4 µM PKH67 during 4 min. Then, 300 µL 1 % BSA were added to bind the excess PKH67 dye. Finally, the EVs were ultracentrifuged at 100 000 x g during 1 h 45 min, and washed twice by ultracentrifugation. Samples without EVs or, with EVs but without PKH67, were also prepared following the same steps to be used as negative controls. For microscopy observation of EV uptake by hepatocytes, cells were seeded on glass coverslips and treated with 5 µg/mL PHK67 labelled-EVs (PKH67-EVs) during 24 hours. After treatment, cells were fixed in 4 % paraformaldehyde for 20 min, washed with PBS 1X. Slides were then viewed using a confocal fluorescence microscope LEICA DMI 6000 CS (Leica Microsystems, Wetzlar, Germany) equipped with a 63× objective. A quantification by spectrophometry was also performed. Approximatively 1.5 million of hepatocytes were treated with 5 µg/mL PHK67-EVs for 24 hours. After treatment, cells were washed in PBS, centrifuged 5 min at 800 x g, resuspended in 200 µL PBS and finally lyzed by sonication. Two hundred microliters of cell lysates were then transferred to 96-well plate and

the PKH67 fluorescence was measured at 502 nm by spectrophotometry using a Perkin Elmer Enspire 2300 multilabel reader (Perkin Elmer, USA). PKH67 fluorescence in cells was normalized by the protein quantity.

2.5. Cell death evaluation of recipient hepatocytes

After treatment by hepatocyte-derived EVs, cells were tested for both apoptotic and necrotic cell death. Apoptotic cells were identified by chromatin condensation and morphological changes in the nucleus using the blue-fluorescence chromatin dye Hoechst 33342, while necrotic cells were evidenced by the SYTOX®Green nucleic acid stain, only permeant to cells with compromised plasma membranes. Briefly, WIF-B9 and primary rat hepatocytes were stained at 37 °C with 175 nM SYTOX®Green and also with 50 µg/mL and 100 µg/mL Hoechst 33342 for 20 and 30 min, respectively. Apoptotic and necrotic cells were then counted using a fluorescence microscope (Axio Scope A1, ZEISS, Marly le Roi, France); 400 cells in total were examined for each condition.

In order to further identify cell death mode, the caspase-3/7 activity assay was performed. Cells were lysed in the caspase activity buffer as previously described [27]. Eighty micrograms of protein were thus incubated with 80 µM DEVD-AMC for 2 hours at 37 °C. Caspase-mediated cleavage of DEVD-AMC was evaluated by spectrofluorimetry (Spectramax Gemini; Molecular Devices, San Jose, California, United States) using 380 nm excitation and 440 nm emission wavelengths.

2.6. Determination of organelle alteration

Electron microscopy of recipient hepatocytes. Ultrastructure changes of recipient WIF-B9 cells were visualized by transmission electron microscopy. After 24 hour-exposure to EVs, hepatocytes were rinsed with 0.15M cacodylate buffer, pH 7.4 and fixed by drop-wise

addition of glutaraldehyde (2.5%) in 0.15M cacodylate buffer, for 1 hour. They were then washed with 0.15M cacodylate buffer and postfixed with 1.5% osmium tetroxide solution containing 1.5% potassium ferrocyanide for 1 hour. Samples were first washed with cacodylate buffer then with water, stained with 1% uranyl acetate for 1 hour and washed again. Next, samples were dehydrated with graded alcohol series following standard procedure prior to inclusion in Epon-Araldite-DMP30 resin (polymerized at 60°C for 48 hours). Sections (0.5 µm) were cut on a Leica UC7 microtome (Leica Microsystems, Wetzlar, Germany) and stained with toluidine blue. Ultrathin sections (80 nm) were obtained and mounted onto copper grids. Sample examination was performed with a JEOL 1400 transmission electron microscope (Jeol Co, Tokyo, Japan) operated at 120 kV and images were digitally captured with an Orius 1000 Gatan Camera (Gatan Ametek, Pleasanton, USA).

Fluorescence microscopy of lysosomes. Lysosomes were labeled by LysoTracker red, a red acidotropic fluoroprobe. After treatment with EVs, hepatocytes, seeded on glass coverslips, were incubated with 1 µM LysoTracker in the culture medium, at 37 °C for 1 h (WIF-B9 hepatocytes) or for 10 min (primary rat hepatocytes). After labelling, cells were fixed in 4 % paraformaldehyde for 20 min, washed with PBS. Slides were then viewed using a confocal fluorescence microscope LEICA DMI 6000 CS (Leica Microsystems, Wetzlar, Germany) equipped with a 40X objective.

Measurement of lysosomal pH. Adapted from a previous paper [41], changes in lysosomal pH were analyzed using the fluorescent ratiometric probe LysoSensor Yellow/Blue DND-160, which exclusively localizes within the lysosomes. The LysoSensor dye emits blue fluorescence in neutral environments, but switches to yellow fluorescence in more acidic environments. After treatment with EVs, hepatocytes, seeded on a 96-well plate, were incubated with 1 µM LysoSensor for 2 min at 37°C. As a positive control of lysosomal alkalinization, some hepatocytes were treated, for 30 min prior to LysoSensor incubation, with 50 nM

bafilomycin A1, a known inhibitor of lysosomal H^+-ATPase (also known as V-ATPase). In parallel, a pH calibration curve was generated. Cells were incubated 2 min at 37°C with 1 µM LysoSensor and then 10 min at 37°C with buffered solutions at pH 4, 5, 6 or 6.5 containing 125 mM KCl, 25 mM NaCl, 10 µM monensin, 10 µM nigericin and 25 mM 2-[N-morpholino] ethanesulfonic acid (MES). Finally, using a Perkin Elmer Enspire 2300 multilabel reader (Perkin Elmer, USA), fluorescence was measured at 440 nm and 540 nm.

2.7. Oxidative stress measurement in hepatocytes

ROS production. Intracellular ROS production was evaluated using dihydroethidium (DHE), as previously described [33]. Briefly, after treatment by hepatocyte-derived EVs, recipient cells were incubated with 25 µM DHE for 1 h at 37°C. Fluorescence (Ex 396 nm/Em 580 nm) was recorded using a microplate reader (EnSpire Multimode 2300 Plate Reader, Perkin Elmer, Waltham, United States). Results were given as relative fluorescence units (RFU)/µg protein.

Analysis of lipid peroxidation. Lipid peroxidation was measured using the fluoroprobe C11-BODIPY$^{581/591}$ (4,4-difluoro-5- [4-phenyl-1,3-butadienyl] -4- bora-3a,4a-diaza-s-indacine-3-undecanoic acid), as previously described [28]. C11-BODIPY$^{581/591}$, which incorporates into cell membranes, shifts from red to green fluorescence upon oxidation. Briefly, cells were incubated with 10 µM C11-BODIPY$^{581/591}$ for 1 h at 37°C. Then, fluorescence was recorded by a SpectraMax Gemini spectrofluorimeter (Molecular Devices Sunnyvale, United States) using two pairs of wavelengths to measure the amount of reduced (λex 590 nm, λem 635 nm) and oxidized probe (λex 485 nm, λem 535 nm). Lipid peroxidation was then quantified by calculating the ratio of oxidized probe/ total probe (oxidized + reduced probe).

Low-molecular-weight iron content. Measurement of intracellular low molecular weight (LMW) iron was based upon the capacity of deferiprone to chelate only LMW iron and

to give a paramagnetic chelate, which can be directly detectable by electron paramagnetic resonance in whole hepatocytes, as previously described [42].

Mitochondrial free iron. Free iron content specifically located in mitochondria was detected using the cell-permeable fluorescent probe Mito-FerroGreen, while mitochondria themselves were visualized by staining with the fluorescent probe MitoTracker red FM.

After treatment with EVs, hepatocytes seeded on glass coverslips were washed with PBS and then incubated with 50 nM MitoTracker red FM and 5 µM Mito-FerroGreen in PBS, at 37 °C for 30 min. After labelling, cells were washed with PBS. Slides were then viewed using a confocal fluorescence microscope LEICA DMI 6000 CS (Leica Microsystems, Wetzlar, Germany) equipped with a 40X objective. Mitochondrial iron content was quantified, cell by cell, by the relative ratio of green over red fluorescence; 100 cells in total were examined for each condition.

2.8. Cytochrome P450 1 activity.

CYP1 activity was estimated by the ethoxyresorufin O-deethylase (EROD) assay that relies on the conversion of ethoxyresorufin into resorufin by CYP1 enzymes. Rapidly, after treatment, cells were incubated with 1.5 mM salicylamide (inhibitor of phase II-conjugating enzymes) and 5 µM ethoxyresorufin. Fluorescence of resorufin (excitation at 544 nm and emission at 584 nm) was monitored for 30 min at 37°C using a microplate reader (EnSpire Multimode 2300 Plate Reader, Perkin Elmer, Waltham, United States). EROD activity was expressed as pg resorufin per min and mg protein.

2.9. Statistical analysis

Values are presented as means ± standard deviation from at least three independent experiments. Statistical analyses were performed using one-way analysis of variance (ANOVA)

followed by a Newman-Keuls post-test. Significance was accepted at $p<0.05$. All statistical analyses were performed using GraphPad Prism5 software (San Diego, United States).

3. RESULTS

3.1. PAH treatment of hepatocytes induces a release of EVs depending on oxidative stress.

BP was previously reported as capable of increasing ROS generation and lipid peroxidation in liver epithelial cells [28], primary rat hepatocytes [27] and WIF-B9 hepatocytes [33] leading to cell death. Therefore, we decided to evaluate the ability of the three selected PAHs to generate oxidative stress in WIF-B9 and primary rat hepatocytes. As expected, BP treatment caused an increase of ROS production and consequent lipid peroxidation after 72 hours of exposure in WIF-B9 hepatocytes (Figure 1A) or after 18 hours in primary rat hepatocytes (Figure 1B). Similar results were obtained with DBA and PYR (Figures 1A and 1B). Using thiourea, a ROS scavenger, and vitamin E, a free radical chain breaking antioxidant, oxidative stress was demonstrated to be involved in PAH-induced cell death (Figures 1C and 1D).

Given that oxidative stress has been demonstrated as inducing EV release in order to protect the producer cells from oxidative damages [43], we examined the effect of antioxidants, *i.e.* thiourea or vitamin E, on the EV release by PAH-treated hepatocytes. As described in Materials and Methods, EVs were isolated from the cell culture media by differential ultracentrifugation and quantified by NTA. Antioxidants significantly reduced the increase in EV release induced by all PAHs (Figures 1E and 1F), thus indicating a role for PAH-induced oxidative stress in EV release by hepatocytes.

3.2. EVs derived from PAH-treated hepatocytes are enriched in proteins related to oxidative stress.

As oxidative stress was involved in the release of EVs upon PAH exposure, this release was proposed as a cellular protective mechanism against oxidative stress by taking away deleterious molecules. Therefore, we decided to look for several proteins related to oxidative stress in EVs [43–46]. First, we examined the changes in the expression levels of NADPH oxidase subunits, gp91-phox (Figures 2A and 2B) and p47-phox (Figures 2C and 2D). Both NADPH oxidase subunits were higher in EVs derived from PAH-treated hepatocytes (PAH-EVs) than in EVs derived from untreated hepatocytes (CTRL-EVs). It is noteworthy that two bands were obtained for the p47-phox regulatory subunit. This could be ascribed to the phosphorylation of this subunit, thus suggesting a stronger activation of NADPH oxidase in PAH-EVs. Second, we explored protein expression of a subunit of ferritin, a storage protein of low-molecular-weight iron (LMW iron). This iron species is known to trigger oxidative stress by catalyzing the formation of a highly reactive free radical, the hydroxyl radical, *via* Fenton or Haber-Weiss reaction. Expression of both ferritin subunits, the ferritin light chain (FTL) and the ferritin heavy chain (FTH), was found to be markedly increased in PAH-EVs from both WIF-B9 and primary hepatocytes (by approximately 60-70 % for FTL, 30-60 % for FTH from WIF-B9 hepatocytes and 100 % for FTH from primary hepatocytes) (Figures 2E-2H). Then, observing by cryo-electron microscopy the ultrastructure of EVs derived from WIF-B9 hepatocytes, large dense structures were found in EVs (Figure 3A, white arrows). These structures may be assimilated to large protein complexes and have been suggested by Truman-Rosentsvit (2018) ~~as~~ to be typical ferritin-iron cores [47]. Interestingly, PAH-EVs contained more of those structures (Figure 3A), thus confirming the results obtained by western-blotting. In order to test a possible elevation of iron within the PAH-EVs, we measured iron atom levels in EVs by electron microscopy coupled with an Energy Dispersive X-Ray Spectroscopy (EDS)

analyser. This technique allows a characterization of the elemental composition of an analysed volume. Levels of iron atom were increased in PAH-EVs compared to CTRL-EVs (Figure 3B). It is noteworthy that iron atom was the only one with significantly modified levels in EVs when hepatocytes were treated by PAHs (Supplementary Figure S2). Interestingly, alongside the release of ferritin in EVs, a decrease in LMW iron was detected at 96 hours of exposure to BP, after a transient increase at 24 hours (Supplementary Figure S3). Those results collectively illustrated that PAH-EVs were enriched in iron most probably stored in ferritin complexes.

3.3. EV released by PAH-treated parent hepatocytes can induce oxidative stress and related damages in recipient hepatocytes

Due to their content in pro-oxidant components such as NADPH oxidase and iron, PAH-EVs may transfer them in recipient hepatocytes. NADPH oxidase generates superoxide anion radical that can lead to the formation of hydrogen peroxide. Iron catalyzes the Fenton reaction that used hydrogen peroxide to produce the highly oxidant hydroxyl radical. Therefore, we wondered whether PAH-EVs could promote oxidative stress and hence harmful processes in recipient hepatocytes. For this purpose, WIF-B9 or primary rat hepatocytes were treated by PAH-EVs in comparison with CTRL-EVs for 24 or 18 hours, respectively. CTRL-EVs did not induce any significant changes in ROS levels compared to hepatocytes without treatment by EVs (Figure 4A and 4B). At the opposite, PAH-EVs increased the ROS levels compared to CTRL-EVs both in WIF-B9 and primary rat hepatocytes (Figures 4A and 4B), thus resulting in a lipid peroxidation of recipient hepatocytes (Figures 4C and 4D).

Consequently, we decided to search for oxidative damages of hepatocytes such as mitochondrial alteration and cell death. In WIF-B9 hepatocytes, mitochondrion ultrastructure was observed by transmission electron microscopy. When compared to CTRL-EV exposure, PAH-EV treatment induced a swelling of mitochondria (Figure 5) and an overall increase in

mitochondrion size (Supplementary Table S2). Mitochondria would also undergo cristae alterations (Figure 5, white arrows) as well as fusion (Figure 5, white asterisks) and fission (Figure 5, solid black arrows) processes. These observations indicated alterations of mitochondria structure, suggestive of a possible ongoing cell death process.

Cell death was therefore estimated by Hoechst 33342 and Sytox®Green staining in order to determine by fluorescent microscopy the number of apoptotic and necrotic hepatocytes. Compared to untreated hepatocytes, cells exposed to CTRL-EVs did not exhibit any significant increase in apoptosis. In contrast, PAH-EVs led to a significant increase (by ≈ 100%) in the number of apoptotic cells for both WIF-B9 (Figure 6A) and primary rat (Figure 6B) hepatocytes. Apoptotic cell death was accompanied by a significant increase in caspase 3/7 activity in both hepatocyte types (by ≈ 50%) (Figures 6C and 6D). Neither CTRL-EVs nor PAH-EVs changed the number of necrotic cells (data not shown). Finally, using the antioxidants, *i.e.* thiourea and vitamin E, PAH-EVs-induced cell death was prevented (Figures 6E and 6F), suggesting a role for oxidative stress in this process.

3.4. PAH-EV-induced apoptosis of recipient hepatocytes is dependent on EV endocytosis and consecutive lysosome permeabilization

In order to understand how PAH-EVs could induce oxidative stress and hence apoptosis of recipient hepatocytes, we first decided to determine whether EVs were internalized by recipient cells. Indeed, uptake of EVs is generally necessary to obtain an effect on recipient cells [48]. The internalization of CTRL-EVs was tested after labelling of EVs with the lipophilic fluorochrome PKH-67. A transfer of PKH67 green fluorescence was observed indicating the EV incorporation within the recipient hepatocytes (Figure 7A, left panel). We next quantified spectrophotometrically this PKH67-EV uptake. Thus, it appears that uptake of PAH-EVs was significantly increased as compared to CTRL-EVs (+50 %) (Figure 7A, right panel). Note that

the fluorescence of PKH67-EV was more specifically localized around the nucleus, thus suggesting an EV presence in lysosomes and hence a possible EV uptake *via* the intracellular vesicular traffic along the endocytic route (Figure 7A, left panel).

Therefore, in order to check the possibility that EV could reach lysosomes, we investigated various mechanisms of EV engulfment by WIF-B9 hepatocytes; to do so, we used cytochalasin B (CyB) and wortmannin (Wort), two inhibitors of endocytosis and phagocytosis, or methyl-β-cyclodextrin (MCD), an inhibitor of a particular endocytosis dependent on lipid rafts. This latter endocytosis type was investigated because lipid rafts (*i.e.* cholesterol-enriched microdomains) have been shown to be involved in BP-induced apoptosis of liver epithelial cells [49] and of primary rat hepatocytes [27]; also an increase in cholesterol content has been previously described in PAH-EVs [23].

In this study, MCD affected neither CTRL-EV nor PAH-EV uptake (Figure 7A, right panel), thus ruling out any possible implication of lipid rafts in EV uptake. In contrast, the reduction in uptake of both CTRL-EVs and PAH-EVs by CyB and Wort (Figure 7A, right panel) highlighted the involvement of endocytosis or phagocytosis in this process. Finally, the same compounds were also tested on PAH-EV-induced apoptosis of recipient hepatocytes. Similarly, only CyB and Wort protected from apoptosis both WIF-B9 (Figure 7B) and primary rat (Figure 7C) hepatocytes, thus suggesting the key role of endocytosis or phagocytosis. These mechanisms of EV uptake therefore supported our assumption that hepatocyte-derived EVs could reach lysosomes within recipient hepatocytes following the classical vesicular traffic *via* endosomes.

We then hypothesized that the accumulation of EVs in lysosomes could alter those organelles leading to cell death. Using bafilomycin A1 (BAF), a selective inhibitor of V-ATPase, in order to reduce lysosome acidity and hence lysosomal hydrolase activity, the PAH-EVs-induced apoptosis of recipient hepatocytes was significantly decreased both in WIF-B9

(Figure 7B) and primary rat (Figure 7C) hepatocytes. In addition, bafilomycin was able to protect from mitochondrial damages (Supplementary Figure S4). Thus, lysosomes appeared as a key organelle in the development of PAH-EV-induced cell death. In this context, we questioned about possible alterations of lysosomes when hepatocytes were exposed to PAH-EVs. First, the red fluorescent probe Lysotracker Red DND-99, which specifically localizes in lysosomes, was used in both WIF-B9 (Figure 8A) and primary rat (Figure 8B) hepatocytes. PAH-EVs caused an increase in lysosome size or a diffusion of fluorescence throughout the whole cell, reflecting a possible lysosome membrane permeabilization in recipient hepatocytes (Figures 8A and 8B). CTRL-EVs do not alter lysosome fluorescence unlike PAH-EVs. Second, to support those observations, lysosome ultrastructure of WIF-B9 hepatocytes was examined by transmission electron microscopy. After PAH-EVs treatment, an increase in lysosome size was also observed (Figure 8C) and measured (Supplementary Table S3). Additionally, hepatocytes exposed to PAH-EVs displayed lysosome membrane permeabilization characterized by a rupture of the lysosome membrane and a visible leak of content (Figure 8C, white arrows).

Since alteration of lysosome membranes have been reported to affect V-ATPase and hence intraluminal pH [50], we measured lysosome pH using the LysoSensor Yellow/Blue DND-160 probe. A 0.2 increase in pH was found (Supplementary Figure S5) and ascertained the alteration of lysosome membrane.

Overall, these results demonstrated that PAH-EVs targeted lysosomes causing a membrane permeabilization and subsequent cell death.

3.5. The pro-oxidant components of EVs, NADPH oxidase and iron, could be involved in PAH-EV-induced apoptosis of recipient hepatocytes

Since PAH-EVs are enriched in proteins related to oxidative stress, such as NADPH oxidase and ferritin, their accumulation in lysosomes of recipient hepatocytes could participate to the alteration of those organelles and hence to apoptosis. To test this hypothesis, we first used two LMW-iron chelators, *i.e.* desferrioxamine and deferiprone. Whereas deferiprone chelates iron in all cell compartments, desferrioxamine is endocytosed and transported to lysosomes, making it a lysosome-specific iron chelator. The PAH-EVs-induced death of recipient WIF-B9 and primary rat hepatocytes was significantly attenuated by deferiprone or desferrioxamine (Figures 7B and 7C). Additionally, the use of either chelator on recipient WIF-B9 hepatocytes limited the PAH-EV-induced lysosome membrane permeabilization (Supplementary Figure S6). Finally, BP-EVs also significantly increased free iron in mitochondria (Figure 9); such an increase was reduced by the lysosome-specific iron chelator, desferrioxamine. Logically, desferrioxamine also protected from PAH-induced mitochondria alterations (Supplementary Figure S4). Altogether, these results suggested that LMW-iron overload in lysosomes is implicated in alterations of those organelles consequently leading to mitochondrial damages and cell death. In line with this, inhibition of NADPH oxidase by apocynin prevented the apoptosis induced by exposure to PAH-EVs in recipient hepatocytes (Figures 7B and 7C).

As BP has already been described to induce oxidative stress and lysosome permeabilization by its own metabolism [51] [27] , one might argue that the above effects could be due to the presence of PAHs in EVs, thereby triggering oxidative stress in the recipient hepatocytes. In order to discard such a mechanism, we measured EROD activity, as an indicator of CYP1 activity. Indeed, the CYP1 enzymes, that are involved in the metabolism of BP and DBA, are known to exhibit a high increase in activity in BP- or DBA-treated hepatocytes due to an elevation of their mRNA expression [23]. Here, CYP1 activity in recipient hepatocytes

was not increased upon exposure to PAHs-EVs (Supplementary Figure S7), thus suggesting that PAHs were not, or in a very negligible quantity, transferred to recipient cells through EVs.

4. DISCUSSION

A growing body of evidences supports the major role of EVs as players of cell communication for the pathogenesis of liver diseases. Yet, nothing is known about their possible involvement in the onset of a key process in the course of liver diseases, namely oxidative stress of the parenchymal hepatic cells. Here, we report, for the first time in hepatocytes and also in the context of exposure to environmental contaminants, that EVs are able to trigger oxidative damages in healthy recipient cells through a requisite internalization of EVs. Thus, the only two published studies, about exposure of hepatocytes to EVs and a possible related oxidative stress, have limited their results to the evaluation of increased ROS levels [52,53]. In our work, in addition to ROS production in recipient hepatocytes, exposure to EVs was demonstrated to trigger lipid peroxidation that in turn caused cell death. In addition, as previously reported for ethanol [54] or ischemia-reperfusion [53], PAHs, by inducing oxidative stress in the producer hepatocytes, promoted EV release. This therefore suggests that oxidative stress is critical, in the context of PAH hepatotoxicity, for both EV release and EV-induced cell death.

In order to understand the mechanisms by which only PAH-EVs could induce oxidative damages in recipient hepatocytes, the specific content of these EVs with regards to compounds related to oxidative stress was compared to CTRL-EV content. Indeed, PAH-induced oxidative stress was clearly identified as the trigger of EV release by the parent hepatocytes. Such an oxidation within the producer cell has been described to promote EV release by various mechanisms [43,55]. When studied, such a release is recurrently proposed as a protective mechanism to discard harmful molecules such as oxidized proteins, mtDNA, phospholipids and

ROS production systems [43–46]. In our present work, NADPH oxidase, an enzyme that produces the free radical superoxide anion, was shown, for the first time in hepatocyte-derived EVs, to be more strongly expressed when producer hepatocytes exhibited an oxidative stress. Regarding other physiopathological conditions such as sepsis or inflammation, an increase in NADPH oxidase expression has also been reported in EVs isolated from bloodstream cells, which also exhibited an elevation of ROS levels [56,57]. Taken altogether, those results thus further support the possible role of EVs to protect the producer cells from oxidative stress. It is noteworthy that Gambim (2007) and Janizewski (2004) also showed that the NADPH oxidase of EVs was functional [56,57].

Expression of another protein related to oxidative stress, namely ferritin, was investigated in PAH-EVs. Recently, it was demonstrated that an important pathway for iron-loaded ferritin secretion occurred through the specialized smaller EV types, that is, exosomes [47]. In our models, exosomes were previously shown to be the main EV type [23]. The ferritin protein complex composed of 24 heavy and light subunits is able to store up to 4500 atoms of the iron element in a nontoxic form from which iron could be released to trigger oxidative damages. Here, the ferritin light subunit was found to be more expressed in PAH-EVs than in CTRL-EVs. In contrast to NADPH oxidase expression in EVs, such an elevation of ferritin light subunit has already been described in EVs released by stressed primary rat hepatocytes [58]. However, so far, authors have not checked a possible co-precipitation of free ferritin with EVs during their ultracentrifugation isolation procedure. In our study, cryo-electron microscopy ascertained the increased presence in PAH-EVs of large dense structures, similar to the typical ferritin-iron cores identified in macrophage EVs [47]. Furthermore, for the first time in EVs released by cells exposed to oxidative stress, an elevation of the levels of iron atom was uncovered by EDS microscopy in PAH-EVs, in accordance with the increase in expression of the iron storage protein ferritin. This supports the assumption by Truman-Rosentsvit (2018) that

secretion of ferritin *via* exosomes could be an export of ferric iron [47]. This release of iron *via* EVs could be related once again to a mean for the hepatocytes to discard harmful molecules capable of inducing oxidative stress and cell death. Indeed, Brown *et al.* (2019) [59] have evidence a possible resistance towards ferroptosis, a new cell death type recently considered for NASH [60], by the way of an iron expulsion in EVs, more specifically in exosomes. Ferroptosis is an iron-dependent, necrosis-like programmed cell death characterized by the accumulation of lipid reactive oxygen species, and hence inhibited by lipophilic antioxidant [61,62]. In our model of WIB-B9 hepatocytes exposed to BP, a transient increase in LMW iron levels has been demonstrated, by electron resonance spectroscopy, at an early time point (24 h) followed by a significant decrease later on (96 h). In addition, the lipophilic antioxidant, vitamin E inhibited the release of EVs. Both those results lead us to suggest that an onset of ferroptosis might be triggered by BP, but would be stopped by the release of exosomes containing iron-loaded ferritin. To sum up, it appears that hepatocytes when submitted to oxidative stress, can release harmful species *via* EVs in order to protect themselves.

However, EVs loaded with such harmful species could then be engulfed by neighboring hepatocytes. Regarding that point, hepatocytes exposed to PAH-EVs were thus demonstrated to sustain oxidative stress leading to cell death, provided that those EVs were internalized in the recipient hepatocytes. This uptake was more important with PAH-EVs than CTRL-EVs. This could be ascribed to their difference in composition formerly reported, notably the increase in cholesterol of PAH-EVs [23]. Indeed, a cholesterol enrichment of surfaces can promote cell adhesion [63,64]. Binding of EVs to recipient cells is now recognized to facilitate subsequent endocytosis [48,65]. EVs derived from hepatocytes submitted to other types of stress such as heat shock [66] or ethanol exposure [54] have also been described to be internalized, but without indicating the prerequisite of an EV engulfment to obtain inflammation or apoptosis of the recipient hepatocytes, respectively. This requirement of an EV uptake is actually decisive to

explain why PAH-EVs but not CTRL-EVs were able to induce oxidative stress in recipient hepatocytes. Indeed, when endocytosed, EVs containing harmful cargoes, can go along the classical pathway of intracellular vesicular traffic to reach lysosomes [65,67]. Up to now, the only relationship between lysosomes and EVs, reported in literature, has dealt with a possible increase in EV release due to lysosome alteration [68,69]. Here, the accumulation of PAH-EVs in lysosomes led to a structural alteration of lysosomes, especially a lysosomal membrane permeabilization, an event well-known as being involved in several types of cell death, including apoptosis [50]. To our knowledge, it is the first time, thanks to the use of bafilomycin A1, an inhibitor of V-ATPase and hence of hydrolase activity, that EVs were found to trigger cell death *via* lysosomal alteration. It is noteworthy to consider that protease leakage from lysosome [50] and lysosomal alkalinization [70], can induce downstream mitochondrial damages, but also ROS generation and caspase 3/7 activation. Thus, we also demonstrate for the first time that EVs, notably PAH-EVs, can induce major structural damages of mitochondria such as swelling and cristae alterations. These results are in accordance with the increase in mitochondrial permeability previously found in hepatocytes treated by circulating EVs from injured mice [53]. Interestingly, mitochondrial fusion and fission, considered as adaptive responses towards severe mitochondrial stress [71,72], might possibly occur in hepatocytes treated by PAH-EVs. Those processes, notably fission, are known to lead to apoptosis depending on the context [73]. It is also interesting to emphasize that, in a context of excessive production of ROS, mitochondria are well-known to constitute a favorite target [74,75].

It was particularly striking that EV cargoes (ferritin and NADPH oxidase), carried away from the parent cells to protect themselves from oxidative stress, would be responsible for lysosome alterations in healthy recipient hepatocytes. Precisely, an oxidative reaction, known to occur in the acidic and hydrolase-enriched lysosome lumen [76], could be triggered by those cargoes. Thus, degradation of ferritin by lysosome hydrolases could provide LMW iron species

involved in the catalysis of the Fenton reaction, that converts hydrogen peroxide to the highly oxidant hydroxyl radical. The latter can then cause lipid peroxidation of lysosome membranes and consecutive lysosome membrane permeabilization. The use of specific lysosomal iron chelator and NADPH oxidase inhibitor has led us to show the involvement of EV cargoes, more precisely ferritin and NADPH oxidase, in PAH-EVs-induced apoptosis of the recipient hepatocytes. While it is the first time that such a route for iron entry and related damage effects is proposed, the participation of NADPH oxidase to apoptosis has previously been reported in endothelial and vascular smooth muscle recipient cells exposed to circulating EVs [56,57]. However, no real explanation of the mechanism involved in the apoptosis induction was provided by those authors. We now propose that NADPH oxidase carried by EVs could be a source of superoxide anion and hence hydrogen peroxide to promote, with iron derived from ferritin, the Fenton reaction needed to induce lysosomal membrane permeabilization (Figure 10).

Finally, iron appeared to have a pivotal role in the process of cell killing by EVs. Indeed, it can also be found in mitochondria of hepatocytes treated by BP-EVs after translocation from lysosomes. An iron translocation from lysosomes to mitochondria has already been described in several types of hepatocyte attack such as ischemia-reperfusion [77], oxidative stress [78] or drug intoxication [79]), but we show, for the first time, that it can also be related to an EV endocytosis. In all cases previously reported [77–79], this iron overload of mitochondria was responsible for mitochondrial ROS formation and permeability transition, and also apoptosis.

It could be confusing to consider EVs as key actors in the progression of PAH-induced oxidative stress leading to cell death, since hepatocytes exposed to those toxicants release EVs loaded with pro-oxidant compounds, likely to reduce the intensity of the damage in the parent cells. Thus, the increase in lipid peroxidation for PAH-exposed hepatocytes was restricted to only 35 %. However, these EVs were able to induce oxidative stress in healthy untreated

hepatocytes. To really appreciate the significance of such an effect, it is important to place this EV release in the particular context of the liver architecture, notably the hepatic lobule, and PAH exposure. First, the flow of blood entering into the lobules from the portal nodes towards the central vein through sinusoidal blood vessels lining hepatocytes contributes to a zonation of the liver. For instance, the pericentral AhR expression [80] and induction of CYP1 enzymes [81] result in increased exposure of the pericentral hepatocytes to toxic intermediates. The possible release of EVs by those hepatocytes into the bile flow [82] that circulate in the opposite direction of the blood flow could thus contribute to the spatial propagation of the PAH toxicity to healthy hepatocytes located in other zones notably in periportal zone. Second, another issue worth stressing is that human PAH exposure can be an environmental intermittent exposure, but EV release due to PAH exposure can propagate the potential hepatotoxicity over a period of several days even in the absence of PAHs. Therefore, EVs create a vicious cycle, thereby aggravating oxidative stress by a spatio and temporal way.

5. Conclusion

The present study reports, for the first time, that EVs released after PAH exposure can mediate lysosome membrane permeabilization of recipient hepatocytes, thereby leading to oxidative stress and ultimately apoptosis. Considering all the present results, we can suggest that the EVs released in the extracellular environment by hepatocytes, possibly protecting themselves from oxidative damage by carrying away deleterious components, could be transferred with their harmful cargoes to neighboring or even distant healthy hepatocytes and induce oxidative stress. Thus, EV cargoes, notably iron and NADPH oxidase, appeared as critical for both EV release and EV-induced oxidative damage. To conclude, hepatocyte-derived EVs could play a key role in the pathogenesis of liver diseases especially in the field of toxicant-associated oxidative stress.

Acknowledgements :

We thank the animal house platform ARCHE (SFR Biosit, Rennes, France) and Laurence Bernard-Touami for her assistance.

Funding :

This study was financially supported by the "Programme Environnement-Santé-Travail" of Anses with the funding from ITMO cancer in the context of the Cancer Plan 2014-2019 [EST-2016/1/31], and by the Cancéropôle Grand Ouest/Région Bretagne (CONCERTO project). Nettie van Meteren is recipient of a doctoral fellowship from the French Ministry for Higher Education and Research.

REFERENCES

[1] M. Yáñez-Mó, P.R.-M. Siljander, Z. Andreu, A. Bedina Zavec, F.E. Borràs, E.I. Buzas, K. Buzas, E. Casal, F. Cappello, J. Carvalho, E. Colás, A. Cordeiro-da Silva, S. Fais, J.M. Falcon-Perez, I.M. Ghobrial, B. Giebel, M. Gimona, M. Graner, I. Gursel, M. Gursel, N.H.H. Heegaard, A. Hendrix, P. Kierulf, K. Kokubun, M. Kosanovic, V. Kralj-Iglic, E.-M. Krämer-Albers, S. Laitinen, C. Lässer, T. Lener, E. Ligeti, A. Linē, G. Lipps, A. Llorente, J. Lötvall, M. Manček-Keber, A. Marcilla, M. Mittelbrunn, I. Nazarenko, E.N.M. Nolte-'t Hoen, T.A. Nyman, L. O'Driscoll, M. Olivan, C. Oliveira, É. Pállinger, H.A. del Portillo, J. Reventós, M. Rigau, E. Rohde, M. Sammar, F. Sánchez-Madrid, N. Santarém, K. Schallmoser, M. Stampe Ostenfeld, W. Stoorvogel, R. Stukelj, S.G. Van der Grein, M. Helena Vasconcelos, M.H.M. Wauben, O. De Wever, Biological properties of extracellular vesicles and their physiological functions, J. Extracell. Vesicles. 4 (2015) 27066. https://doi.org/10.3402/jev.v4.27066.

[2] M. Simons, G. Raposo, Exosomes – vesicular carriers for intercellular communication, Curr. Opin. Cell Biol. 21 (2009) 575–581. https://doi.org/10.1016/j.ceb.2009.03.007.

[3] G. van Niel, G. D'Angelo, G. Raposo, Shedding light on the cell biology of extracellular vesicles, Nat. Rev. Mol. Cell Biol. 19 (2018) 213–228. https://doi.org/10.1038/nrm.2017.125.

[4] P.B. Devhare, R.B. Ray, Extracellular vesicles: Novel mediator for cell to cell communications in liver pathogenesis, Mol. Aspects Med. 60 (2018) 115–122. https://doi.org/10.1016/j.mam.2017.11.001.

[5] P. Hirsova, S.H. Ibrahim, V.K. Verma, L.A. Morton, V.H. Shah, N.F. LaRusso, G.J. Gores, H. Malhi, Extracellular vesicles in liver pathobiology: Small particles with big impact, Hepatology. 64 (2016) 2219–2233. https://doi.org/10.1002/hep.28814.

[6] K. Sato, L. Kennedy, S. Liangpunsakul, P. Kusumanchi, Z. Yang, F. Meng, S. Glaser, H. Francis, G. Alpini, Intercellular Communication between Hepatic Cells in Liver Diseases, Int. J. Mol. Sci. 20 (2019) 2180. https://doi.org/10.3390/ijms20092180.

[7] I. Garcia-Martinez, N. Santoro, Y. Chen, R. Hoque, X. Ouyang, S. Caprio, M.J. Shlomchik, R.L. Coffman, A. Candia, W.Z. Mehal, Hepatocyte mitochondrial DNA drives nonalcoholic steatohepatitis by activation of TLR9, J. Clin. Invest. 126 (2016) 859–864. https://doi.org/10.1172/JCI83885.

[8] E. Kakazu, A.S. Mauer, M. Yin, H. Malhi, Hepatocytes release ceramide-enriched pro-inflammatory extracellular vesicles in an IRE1α-dependent manner, J. Lipid Res. 57 (2016) 233–245. https://doi.org/10.1194/jlr.M063412.

[9] C.-Y. Liao, M.J. Song, Y. Gao, A.S. Mauer, A. Revzin, H. Malhi, Hepatocyte-derived lipotoxic extracellular vesicle sphingosine 1-phosphate induces macrophage chemotaxis, Front. Immunol. 9 (2018). https://doi.org/10.3389/fimmu.2018.02980.

[10] D. Povero, N. Panera, A. Eguchi, C.D. Johnson, B.G. Papouchado, L. de Araujo Horcel, E.M. Pinatel, A. Alisi, V. Nobili, A.E. Feldstein, Lipid-induced hepatocyte-derived extracellular vesicles regulate hepatic stellate cells via microRNA targeting peroxisome proliferator-activated receptor-γ, Cell. Mol. Gastroenterol. Hepatol. 1 (2015) 646–663.

[11] Y.-S. Lee, S.Y. Kim, E. Ko, J.-H. Lee, H.-S. Yi, Y.J. Yoo, J. Je, S.J. Suh, Y.K. Jung, J.H. Kim, Y.S. Seo, H.J. Yim, W.-I. Jeong, J.E. Yeon, S.H. Um, K.S. Byun, Exosomes derived from palmitic acid-treated hepatocytes induce fibrotic activation of hepatic stellate cells, Sci. Rep. 7 (2017). https://doi.org/10.1038/s41598-017-03389-2.

[12] F. Jiang, Q. Chen, W. Wang, Y. Ling, Y. Yan, P. Xia, Hepatocyte-derived extracellular vesicles promote endothelial inflammation and atherogenesis via microRNA-1, J. Hepatol. 72 (2020) 156–166. https://doi.org/10.1016/j.jhep.2019.09.014.

[13] D. Povero, A. Eguchi, I.R. Niesman, N. Andronikou, X. de Mollerat du Jeu, A. Mulya, M. Berk, M. Lazic, S. Thapaliya, M. Parola, H.H. Patel, A.E. Feldstein, Lipid-induced toxicity stimulates hepatocytes to release angiogenic microparticles that require vanin-1 for uptake by endothelial cells, Sci. Signal. 6 (2013) ra88–ra88. https://doi.org/10.1126/scisignal.2004512.

[14] S. Li, M. Hong, H.-Y. Tan, N. Wang, Y. Feng, Insights into the role and interdependence of oxidative stress and inflammation in liver diseases, Oxid. Med. Cell. Longev. 2016 (2016) 1–21. https://doi.org/10.1155/2016/4234061.

[15] M. Masarone, V. Rosato, M. Dallio, A.G. Gravina, A. Aglitti, C. Loguercio, A. Federico, M. Persico, Role of oxidative stress in pathophysiology of nonalcoholic fatty liver disease, Oxid. Med. Cell. Longev. 2018 (2018) 1–14. https://doi.org/10.1155/2018/9547613.

[16] Z. Chen, R. Tian, Z. She, J. Cai, H. Li, Role of oxidative stress in the pathogenesis of nonalcoholic fatty liver disease, Free Radic. Biol. Med. 152 (2020) 116–141. https://doi.org/10.1016/j.freeradbiomed.2020.02.025.

[17] G. Bodega, M. Alique, L. Puebla, J. Carracedo, R.M. Ramírez, Microvesicles: ROS scavengers and ROS producers, J. Extracell. Vesicles. 8 (2019) 1626654. https://doi.org/10.1080/20013078.2019.1626654.

[18] W. Tan, Y. Zhang, M. Li, X. Zhu, X. Yang, J. Wang, S. Zhang, W. Zhu, J. Cao, H. Yang, L. Zhang, miR-27a-containing exosomes secreted by irradiated skin keratinocytes delayed the migration of unirradiated skin fibroblasts, Int. J. Biol. Sci. 15 (2019) 2240–2255. https://doi.org/10.7150/ijbs.35356.

[19] A. Söderberg, A.M. Barral, M. Söderström, B. Sander, A. Rosén, Redox-signaling transmitted in trans to neighboring cells by melanoma-derived TNF-containing exosomes, Free Radic. Biol. Med. 43 (2007) 90–99. https://doi.org/10.1016/j.freeradbiomed.2007.03.026.

[20] S. Dutta, C. Warshall, C. Bandyopadhyay, D. Dutta, B. Chandran, Interactions between exosomes from breast cancer cells and primary mammary epithelial cells leads to generation of reactive

oxygen species which induce DNA damage response, stabilization of p53 and autophagy in epithelial cells, PLoS ONE. 9 (2014) e97580. https://doi.org/10.1371/journal.pone.0097580.

[21] F.R.M. Stassen, P.H. van Eijck, P.H.M. Savelkoul, E.F.M. Wouters, G.G.U. Rohde, J.J. Briedé, N.L. Reynaert, T.M. de Kok, B.J. Benedikter, Cell type- and exposure-specific modulation of CD63/CD81-positive and tissue factor-positive extracellular vesicle release in response to respiratory toxicants, Oxid. Med. Cell. Longev. 2019 (2019) 1–9. https://doi.org/10.1155/2019/5204218.

[22] B.J. Benedikter, C. Volgers, P.H. van Eijck, E.F.M. Wouters, P.H.M. Savelkoul, N.L. Reynaert, G.R.M.M. Haenen, G.G.U. Rohde, A.R. Weseler, F.R.M. Stassen, Cigarette smoke extract induced exosome release is mediated by depletion of exofacial thiols and can be inhibited by thiol-antioxidants, Free Radic. Biol. Med. 108 (2017) 334–344. https://doi.org/10.1016/j.freeradbiomed.2017.03.026.

[23] N. van Meteren, D. Lagadic-Gossmann, M. Chevanne, I. Gallais, D. Gobart, A. Burel, S. Bucher, N. Grova, B. Fromenty, B.M.R. Appenzeller, S. Chevance, F. Gauffre, E. Le Ferrec, O. Sergent, Polycyclic aromatic hydrocarbons can trigger hepatocyte release of extracellular vesicles by various mechanisms of action depending on their affinity for the aryl hydrocarbon receptor, Toxicol. Sci. 171 (2019) 443–462. https://doi.org/10.1093/toxsci/kfz157.

[24] S.-H. Cherng, S.-L. Hsu, J.-L. Yang, C.-T.R. Yu, H. Lee, Suppressive effect of 1-nitropyrene on benzo[a]pyrene-induced CYP1A1 protein expression in HepG2 cells, Toxicol. Lett. 161 (2006) 236–243. https://doi.org/10.1016/j.toxlet.2005.10.002.

[25] L. Huc, L. Sparfel, M. Rissel, M.-T. Dimanche-Boitrel, A. Guillouzo, O. Fardel, D. Lagadic-Gossmann, Identification of Na+/H+ exchange as a new target for toxic polycyclic aromatic hydrocarbons, FASEB J. 18 (2004) 344–346.

[26] J.-Q. Ma, C.-M. Liu, Z.-H. Qin, J.-H. Jiang, Y.-Z. Sun, Ganoderma applanatum terpenes protect mouse liver against benzo(α)pyren-induced oxidative stress and inflammation, Environ. Toxicol. Pharmacol. 31 (2011) 460–468. https://doi.org/10.1016/j.etap.2011.02.007.

[27] A. Collin, K. Hardonnière, M. Chevanne, J. Vuillemin, N. Podechard, A. Burel, M.-T. Dimanche-Boitrel, D. Lagadic-Gossmann, O. Sergent, Cooperative interaction of benzo[a]pyrene and ethanol on plasma membrane remodeling is responsible for enhanced oxidative stress and cell death in primary rat hepatocytes, Free Radic. Biol. Med. 72 (2014) 11–22. https://doi.org/10.1016/j.freeradbiomed.2014.03.029.

[28] M. Gorria, X. Tekpli, O. Sergent, L. Huc, F. Gaboriau, M. Rissel, M. Chevanne, M.-T. Dimanche-Boitrel, D. Lagadic-Gossmann, Membrane fluidity changes are associated with benzo[a]pyrene-induced apoptosis in F258 cells: protection by exogenous cholesterol, Ann. N. Y. Acad. Sci. 1090 (2006) 108–112. https://doi.org/10.1196/annals.1378.011.

[29] M. Kumar, V.L. Sharma, A. Sehgal, M. Jain, Protective effects of green and white tea against benzo(a)pyrene induced oxidative stress and DNA damage in murine model, Nutr. Cancer. 64 (2012) 300–306. https://doi.org/10.1080/01635581.2012.648300.

[30] J.-H. Park, D. Mangal, A.J. Frey, R.G. Harvey, I.A. Blair, T.M. Penning, Aryl hydrocarbon receptor facilitates DNA strand breaks and 8-oxo-2′-deoxyguanosine formation by the aldo-keto reductase product benzo[a]pyrene-7,8-dione, J. Biol. Chem. 284 (2009) 29725–29734. https://doi.org/10.1074/jbc.M109.042143.

[31] A. Sehgal, M. Kumar, M. Jain, D.K. Dhawan, Combined effects of curcumin and piperine in ameliorating benzo(a)pyrene induced DNA damage, Food Chem. Toxicol. 49 (2011) 3002–3006. https://doi.org/10.1016/j.fct.2011.07.058.

[32] X. Tekpli, M. Rissel, L. Huc, D. Catheline, O. Sergent, V. Rioux, P. Legrand, J.A. Holme, M.-T. Dimanche-Boitrel, D. Lagadic-Gossmann, Membrane remodeling, an early event in benzo[α]pyrene-induced apoptosis, Toxicol. Appl. Pharmacol. 243 (2010) 68–76. https://doi.org/10.1016/j.taap.2009.11.014.

[33] A. Tête, I. Gallais, M. Imran, M. Chevanne, M. Liamin, L. Sparfel, S. Bucher, A. Burel, N. Podechard, B.M.R. Appenzeller, B. Fromenty, N. Grova, O. Sergent, D. Lagadic-Gossmann, Mechanisms involved in the death of steatotic WIF-B9 hepatocytes co-exposed to benzo[a]pyrene and ethanol: a possible key role for xenobiotic metabolism and nitric oxide, Free Radic. Biol. Med. 129 (2018) 323–337. https://doi.org/10.1016/j.freeradbiomed.2018.09.042.

[34] J.-K. Ma, W.F. Saad Eldin, W.R. El-Ghareeb, A.E. Elhelaly, M.H.E. Khedr, X. Li, X.-C. Huang, Effects of pyrene on human liver HepG2 cells: cytotoxicity, oxidative stress, and transcriptomic changes in xenobiotic metabolizing enzymes and inflammatory markers with protection trial using lycopene, BioMed Res. Int. 2019 (2019) 1–10. https://doi.org/10.1155/2019/7604851.

[35] X.-J. Zhang, Z. Shi, J.-X. Lyv, X. He, N.A. Englert, S.-Y. Zhang, Pyrene is a novel Constitutive Androstane Receptor (CAR) activator and causes hepatotoxicity by CAR, Toxicol. Sci. 147 (2015) 436–445. https://doi.org/10.1093/toxsci/kfv142.

[36] C. Biagini, V. Bender, F. Borde, E. Boissel, M.-C. Bonnet, M.-T. Masson, D. Cassio, S. Chevalier, Cytochrome P450 expression—induction profile and chemically mediated alterations of the WIF-B9 cell line, Biol. Cell. 98 (2006) 23–32. https://doi.org/10.1042/BC20050003.

[37] S. Bucher, A. Tête, N. Podechard, M. Liamin, D. Le Guillou, M. Chevanne, C. Coulouarn, M. Imran, I. Gallais, M. Fernier, Q. Hamdaoui, M.-A. Robin, O. Sergent, B. Fromenty, D. Lagadic-Gossmann, Co-exposure to benzo[a]pyrene and ethanol induces a pathological progression of liver steatosis in vitro and in vivo, Sci. Rep. 8 (2018) 5963. https://doi.org/10.1038/s41598-018-24403-1.

[38] EFSA, Polycyclic Aromatic Hydrocarbons in Food - Scientific Opinion of the Panel on Contaminants in the Food Chain, EFSA J. 6 (2008) 724. https://doi.org/10.2903/j.efsa.2008.724.

[39] M. Machala, J. Vondráček, L. Bláha, M. Ciganek, J. Neča, Aryl hydrocarbon receptor-mediated activity of mutagenic polycyclic aromatic hydrocarbons determined using in vitro reporter gene assay, Mutat. Res. Toxicol. Environ. Mutagen. 497 (2001) 49–62.

[40] J. Dubochet, A.W. McDowall, Vitrification of pure water for electron microscopy, J. Microsc. 124 (1981) 3–4. https://doi.org/10.1111/j.1365-2818.1981.tb02483.x.

[41] L. Ma, Q. Ouyang, G.C. Werthmann, H.M. Thompson, E.M. Morrow, Live-cell microscopy and fluorescence-based measurement of luminal pH in intracellular organelles, Front. Cell Dev. Biol. 5 (2017) 71. https://doi.org/10.3389/fcell.2017.00071.

[42] O. Sergent, J.P. Anger, G. Lescoat, N. Pasdeloup, P. Cillard, J. Cillard, EPR determination of low molecular weight iron content applied to whole rat hepatocytes, Cell. Mol. Biol. Noisy--Gd. Fr. 43 (1997) 793–800.

[43] B.J. Benedikter, A.R. Weseler, E.F.M. Wouters, P.H.M. Savelkoul, G.G.U. Rohde, F.R.M. Stassen, Redox-dependent thiol modifications: implications for the release of extracellular vesicles, Cell. Mol. Life Sci. 75 (2018) 2321–2337. https://doi.org/10.1007/s00018-018-2806-z.

[44] C. Borras, C. Mas-Bargues, J. Sanz-Ros, A. Román-Domínguez, L. Gimeno-Mallench, M. Inglés, J. Gambini, J. Viña, Extracellular vesicles and redox modulation in aging, Free Radic. Biol. Med. (2019) S0891584919314169. https://doi.org/10.1016/j.freeradbiomed.2019.11.032.

[45] K. Szabó-Taylor, B. Ryan, X. Osteikoetxea, T.G. Szabó, B. Sódar, M. Holub, A. Németh, K. Pálóczi, É. Pállinger, P. Winyard, E.I. Buzás, Oxidative and other posttranslational modifications in extracellular vesicle biology, Semin. Cell Dev. Biol. 40 (2015) 8–16. https://doi.org/10.1016/j.semcdb.2015.02.012.

[46] C. Yarana, D. St. Clair, Chemotherapy-induced tissue injury: an insight into the role of extracellular vesicles-mediated oxidative stress responses, Antioxidants. 6 (2017) 75. https://doi.org/10.3390/antiox6040075.

[47] M. Truman-Rosentsvit, D. Berenbaum, L. Spektor, L.A. Cohen, S. Belizowsky-Moshe, L. Lifshitz, J. Ma, W. Li, E. Kesselman, I. Abutbul-Ionita, D. Danino, L. Gutierrez, H. Li, K. Li, H. Lou, M. Regoni, M. Poli, F. Glaser, T.A. Rouault, E.G. Meyron-Holtz, Ferritin is secreted via 2 distinct nonclassical vesicular pathways, Blood. 131 (2018) 342–352. https://doi.org/10.1182/blood-2017-02-768580.

[48] L.A. Mulcahy, R.C. Pink, D.R.F. Carter, Routes and mechanisms of extracellular vesicle uptake, J. Extracell. Vesicles. 3 (2014) 24641. https://doi.org/10.3402/jev.v3.24641.

[49] X. Tekpli, L. Huc, O. Sergent, B. Dendelé, M.-T. Dimanche-Boitrel, J.A. Holme, D. Lagadic-Gossmann, NHE-1 relocation outside cholesterol-rich membrane microdomains is associated with its benzo [a] pyrene-related apoptotic function, Cell. Physiol. Biochem. 29 (2012) 657–666.

[50] F. Wang, R. Gómez-Sintes, P. Boya, Lysosomal membrane permeabilization and cell death, Traffic. 19 (2018) 918–931. https://doi.org/10.1111/tra.12613.

[51] M. Gorria, X. Tekpli, M. Rissel, O. Sergent, L. Huc, N. Landvik, O. Fardel, M.-T. Dimanche-Boitrel, J.A. Holme, D. Lagadic-Gossmann, A new lactoferrin- and iron-dependent lysosomal death pathway is induced by benzo[a]pyrene in hepatic epithelial cells, Toxicol. Appl. Pharmacol. 228 (2008) 212–224. https://doi.org/10.1016/j.taap.2007.12.021.

[52] Y.-E. Cho, W. Seo, D.-K. Kim, P.-G. Moon, S.-H. Kim, B.-H. Lee, B.-J. Song, M.-C. Baek, Exogenous exosomes from mice with acetaminophen-induced liver injury promote toxicity in the recipient hepatocytes and mice, Sci. Rep. 8 (2018). https://doi.org/10.1038/s41598-018-34309-7.

[53] N.C. Teoh, H. Ajamieh, H.J. Wong, K. Croft, T. Mori, A.C. Allison, G.C. Farrell, Microparticles mediate hepatic ischemia-reperfusion injury and are the targets of diannexin (ASP8597), PLoS ONE. 9 (2014) e104376. https://doi.org/10.1371/journal.pone.0104376.

[54] Y.-E. Cho, E. Mezey, J.P. Hardwick, N. Salem, D.L. Clemens, B.-J. Song, Increased ethanol-inducible cytochrome P450-2E1 and cytochrome P450 isoforms in exosomes of alcohol-exposed rodents and patients with alcoholism through oxidative and endoplasmic reticulum stress, Hepatol. Commun. 1 (2017) 675–690.

[55] M.C. Larson, C.A. Hillery, N. Hogg, Circulating membrane-derived microvesicles in redox biology, Free Radic. Biol. Med. 73 (2014) 214–228. https://doi.org/10.1016/j.freeradbiomed.2014.04.017.

[56] M.H. Gambim, A.D.O. Do Carmo, L. Marti, S. Veríssimo-Filho, L.R. Lopes, M. Janiszewski, Platelet-derived exosomes induce endothelial cell apoptosis through peroxynitrite generation: experimental evidence for a novel mechanism of septic vascular dysfunction, Crit. Care. 11 (2007) R107.

[57] M. Janiszewski, A.O. do Carmo, M.A. Pedro, E. Silva, E. Knobel, F.R.M. Laurindo, Platelet-derived exosomes of septic individuals possess proapoptotic NAD(P)H oxidase activity: A novel vascular redox pathway*:, Crit. Care Med. 32 (2004) 818–825. https://doi.org/10.1097/01.CCM.0000114829.17746.19.

[58] E. Rodríguez-Suárez, E. Gonzalez, C. Hughes, J. Conde-Vancells, A. Rudella, F. Royo, L. Palomo, F. Elortza, S.C. Lu, J.M. Mato, J.P.C. Vissers, J.M. Falcón-Pérez, Quantitative proteomic analysis of hepatocyte-secreted extracellular vesicles reveals candidate markers for liver toxicity, J. Proteomics. 103 (2014) 227–240. https://doi.org/10.1016/j.jprot.2014.04.008.

[59] C.W. Brown, J.J. Amante, P. Chhoy, A.L. Elaimy, H. Liu, L.J. Zhu, C.E. Baer, S.J. Dixon, A.M. Mercurio, Prominin2 drives ferroptosis resistance by stimulating iron export, Dev. Cell. 51 (2019) 575-586.e4. https://doi.org/10.1016/j.devcel.2019.10.007.

[60] S. Aizawa, G. Brar, H. Tsukamoto, Cell death and liver disease, Gut Liver. 14 (2020) 20–29. https://doi.org/10.5009/gnl18486.

[61] S.J. Dixon, K.M. Lemberg, M.R. Lamprecht, R. Skouta, E.M. Zaitsev, C.E. Gleason, D.N. Patel, A.J. Bauer, A.M. Cantley, W.S. Yang, B. Morrison, B.R. Stockwell, Ferroptosis: an iron-

dependent form of nonapoptotic cell death, Cell. 149 (2012) 1060–1072. https://doi.org/10.1016/j.cell.2012.03.042.

[62] M. Gao, P. Monian, N. Quadri, R. Ramasamy, X. Jiang, Glutaminolysis and transferrin regulate ferroptosis, Mol. Cell. 59 (2015) 298–308. https://doi.org/10.1016/j.molcel.2015.06.011.

[63] J.J. Hwang, S.N. Iyer, L.-S. Li, R. Claussen, D.A. Harrington, S.I. Stupp, Self-assembling biomaterials: Liquid crystal phases of cholesteryl oligo(L-lactic acid) and their interactions with cells, Proc. Natl. Acad. Sci. 99 (2002) 9662–9667. https://doi.org/10.1073/pnas.152667399.

[64] G. Yu, J. Ji, J. Shen, Synthesis and characterization of cholesterol-poly(ethylene glycol)-poly(D,L-lactic acid) copolymers for promoting osteoblast attachment and proliferation, J. Mater. Sci. Mater. Med. 17 (2006) 899–909. https://doi.org/10.1007/s10856-006-0188-5.

[65] T. Tian, Y.-L. Zhu, F.-H. Hu, Y.-Y. Wang, N.-P. Huang, Z.-D. Xiao, Dynamics of exosome internalization and trafficking, J. Cell. Physiol. 228 (2013) 1487–1495. https://doi.org/10.1002/jcp.24304.

[66] Y. Li, X. Zhu, M. Zhang, H. Tong, L. Su, Heatstroke-induced hepatocyte exosomes promote liver injury by activating the NOD-like receptor signaling pathway in mice, PeerJ. 7 (2019) e8216. https://doi.org/10.7717/peerj.8216.

[67] J. Zheng, J. Tan, Y.-Y. Miao, Q. Zhang, Extracellular vesicles degradation pathway based autophagy lysosome pathway, (2019) 14.

[68] L. Alvarez-Erviti, Y. Seow, A.H. Schapira, C. Gardiner, I.L. Sargent, M.J.A. Wood, J.M. Cooper, Lysosomal dysfunction increases exosome-mediated alpha-synuclein release and transmission, Neurobiol. Dis. 42 (2011) 360–367. https://doi.org/10.1016/j.nbd.2011.01.029.

[69] A.M. Miranda, Z.M. Lasiecka, Y. Xu, J. Neufeld, S. Shahriar, S. Simoes, R.B. Chan, T.G. Oliveira, S.A. Small, G. Di Paolo, Neuronal lysosomal dysfunction releases exosomes harboring APP C-terminal fragments and unique lipid signatures, Nat. Commun. 9 (2018) 291. https://doi.org/10.1038/s41467-017-02533-w.

[70] E.A. Assali, D. Shlomo, J. Zeng, E.P. Taddeo, K.M. Trudeau, K.A. Erion, A.H. Colby, M.W. Grinstaff, M. Liesa, G. Las, O.S. Shirihai, Nanoparticle- mediated lysosomal reacidification restores mitochondrial turnover and function in β cells under lipotoxicity, FASEB J. 33 (2019) 4154–4165. https://doi.org/10.1096/fj.201801292R.

[71] J.N. Meyer, T.C. Leuthner, A.L. Luz, Mitochondrial fusion, fission, and mitochondrial toxicity, Toxicology. 391 (2017) 42–53. https://doi.org/10.1016/j.tox.2017.07.019.

[72] A. Picca, F. Guerra, R. Calvani, C. Bucci, M. Lo Monaco, A. Bentivoglio, H. Coelho-Júnior, F. Landi, R. Bernabei, E. Marzetti, Mitochondrial dysfunction and aging: insights from the analysis of extracellular vesicles, Int. J. Mol. Sci. 20 (2019) 805. https://doi.org/10.3390/ijms20040805.

[73] J.-L. Perfettini, T. Roumier, G. Kroemer, Mitochondrial fusion and fission in the control of apoptosis, Trends Cell Biol. 15 (2005) 179–183. https://doi.org/10.1016/j.tcb.2005.02.005.

[74] G. Paradies, V. Paradies, F.M. Ruggiero, G. Petrosillo, Oxidative stress, cardiolipin and mitochondrial dysfunction in nonalcoholic fatty liver disease, World J. Gastroenterol. 20 (2014) 14205. https://doi.org/10.3748/wjg.v20.i39.14205.

[75] A. Mansouri, C.-H. Gattolliat, T. Asselah, Mitochondrial dysfunction and signaling in chronic liver diseases, Gastroenterology. 155 (2018) 629–647. https://doi.org/10.1053/j.gastro.2018.06.083.

[76] A. Terman, T. Kurz, Lysosomal iron, iron chelation, and cell death, Antioxid. Redox Signal. 18 (2013) 888–898. https://doi.org/10.1089/ars.2012.4885.

[77] X. Zhang, J.J. Lemasters, Translocation of iron from lysosomes to mitochondria during ischemia predisposes to injury after reperfusion in rat hepatocytes, Free Radic. Biol. Med. 63 (2013) 243–253. https://doi.org/10.1016/j.freeradbiomed.2013.05.004.

[78] A. Uchiyama, J.-S. Kim, K. Kon, H. Jaeschke, K. Ikejima, S. Watanabe, J.J. Lemasters, Translocation of iron from lysosomes into mitochondria is a key event during oxidative stress-induced hepatocellular injury, Hepatol. Baltim. Md. 48 (2008) 1644–1654. https://doi.org/10.1002/hep.22498.

[79] J. Hu, A. Kholmukhamedov, C.C. Lindsey, C.C. Beeson, H. Jaeschke, J.J. Lemasters, Translocation of iron from lysosomes to mitochondria during acetaminophen-induced hepatocellular injury: Protection by starch-desferal and minocycline, Free Radic. Biol. Med. 97 (2016) 418–426. https://doi.org/10.1016/j.freeradbiomed.2016.06.024.

[80] K.O. Lindros, T. Oinonen, I. Johansson, M. Ingelman-Sundberg, Selective centrilobular expression of the aryl hydrocarbon receptor in rat liver, J. Pharmacol. Exp. Ther. 280 (1997) 506–511.

[81] T. Oinonen, S. Saarikoski, K. Husgafvel-Pursiainen, A. Hirvonen, K.O. Lindros, Pretranslational induction of cytochrome P4501A enzymes by beta-naphthoflavone and 3-methylcholanthrene occurs in different liver zones, Biochem. Pharmacol. 48 (1994) 2189–2197. https://doi.org/10.1016/0006-2952(94)00385-8.

[82] A.I. Masyuk, B.Q. Huang, C.J. Ward, S.A. Gradilone, J.M. Banales, T.V. Masyuk, B. Radtke, P.L. Splinter, N.F. LaRusso, Biliary exosomes influence cholangiocyte regulatory mechanisms and proliferation through interaction with primary cilia, Am. J. Physiol.-Gastrointest. Liver Physiol. 299 (2010) G990–G999. https://doi.org/10.1152/ajpgi.00093.2010.

FIGURE LEGENDS

Figure 1: Oxidative stress in parent hepatocytes is involved in their EV release when exposed to PAHs. (**A, B**) Oxidative stress followed by the evaluation of reactive oxygen species (ROS) production and lipid peroxidation. ROS production was measured by the fluorescence of oxidized dihydroethidium (DHE) (left panel) and lipid peroxidation by the fluorescence of oxidized C11-BODIPY$^{581/591}$ relative to the total fluorescence (oxidized + reduced fluorochrome) (right panel). (**C, D**) Apoptosis estimated by microscopic observation of the number of cells with condensed and/or fragmented chromatin after nuclear staining by Hoechst 33342. (**E, F**) EV release was evaluated by Nanoparticle Tracking Analysis. WIF-B9 (**A, C, E**) and primary rat (**B, D, F**) hepatocytes were exposed or not to 100 nM BP, DBA or PYR for 72 hours and 18 hours, respectively. Untreated cultures were used as controls (CTRL). Some cultures were pre-treated for 30 minutes or not (-) with 6.25 mM thiourea (Th), a ROS scavenger or 100 µM vitamin E (VitE), a free radical chain-breaking antioxidant. Values are given as means ± standard deviation of 3 to 7 independent experiments. Treated *versus* CTRL: ***p<0.001. Th or VitE pre-treated *versus* non pre-treated: #p<0.01.

Figure 2: EVs derived from PAH-treated hepatocytes are enriched in proteins related to oxidative stress. Protein expressions of NADPH oxidase subunits, gp91phox (**A, B**) and p47phox (**C, D**), and of ferritin subunit, the ferritin light chain FTL (**E, F**) and the ferritin heavy chain FTH (**G, H**), were studied in EVs by western blotting. EVs were isolated from WIF-B9 (**A, C, E, G**) and primary rat (**B, D, F, H**) hepatocytes exposed or not to 100 nM BP, DBA or PYR for 72 hours and 18 hours, respectively. Values are given as means ± standard deviation of 3 to 5 independent experiments, except for p47 phox and FTH protein in primary rat hepatocytes, for which only one experiment was performed. Treated *versus* CTRL: **p<0.01; ***p<0.001.

Figure 3: EVs derived from PAH-treated hepatocytes are enriched in iron. (A) Ultrastructure of unstained EVs observed using cryo-electron microscopy. Vitrified samples were loaded to a Technai G2 T20 Sphera electron microscope operating at 200 kV. The white arrows point to dense structures supposed to be iron cores. Note that dense structures apparently outside vesicles are actually disrupted vesicles due to the vitrification process needed for cryo-electron microscopy. **(B)** Iron content of EVs measured using electron microscopy coupled with an Energy Dispersive X-Ray Spectroscopy (EDS) analyzer. EVs were isolated from WIF-B9

hepatocytes exposed or not to 100 nM BP, DBA or PYR for 72 hours. Images of cryo-electron microscopy are representative of 2 independent experiments. For iron content measurement, values are given as means ± standard deviation of 20 to 30 vesicles from 2 independent experiments. Treated *versus* CTRL: *p<0.05; ***p<0.001.

Figure 4: EVs from PAH-treated parent hepatocytes induce oxidative stress in recipient healthy hepatocytes. Oxidative stress was followed by the evaluation of reactive oxygen species (ROS) production (**A, B**) and lipid peroxidation (**C, D**). ROS production was measured by the fluorescence of oxidized dihydroethidium (DHE) and lipid peroxidation by the fluorescence of oxidized C11-BODIPY$^{581/591}$ relative to the total fluorescence (oxidized + reduced fluorochrome). WIF-B9 (**A, C**) and primary rat (**B, D**) healthy hepatocytes were treated or not (no EV) by 5 µg/mL EVs for 24 and 18 hours, respectively. EVs were isolated from WIF-B9 or primary rat parent hepatocytes exposed or not (CTRL-EV) to 100 nM BP (BP-EV), DBA (DBA-EV) or PYR (PYR-EV) for 72 hours and 18 hours, respectively. Values are given as means ± standard deviation of 3 to 7 independent experiments. Treated with EVs *versus* untreated: ***p<0.001.

Figure 5: EVs from PAH-treated parent hepatocytes alter mitochondrial ultrastructure of recipient hepatocytes. (**A)** Mitochondrial ultrastructure. (**B**) Mitochondrial crista ultrastructure. Ultra-thin sections (80 nm) of each sample were observed under transmission electron microscopy (TEM). White arrows, white asterisks and black solid arrows indicate crista alteration, fusion and fission of mitochondria, respectively. WIF-B9 healthy hepatocytes were treated or not (no EV) by 5 µg/mL EVs for 24 hours. EVs were isolated from WIF-B9 hepatocytes exposed or not (CTRL-EV) to 100 nM BP (BP-EV), DBA (DBA-EV) or PYR (PYR-EV) for 72 hours. The images are representative of 2 independent experiments.

Figure 6: EVs from PAH-treated parent hepatocytes induce apoptosis of recipient hepatocytes. Apoptosis was estimated by microscopic observation of the number of cells with condensed and/or fragmented chromatin after nuclear staining by Hoechst 33342 (**A, B, E, F**), and by measuring DEVDase activities of caspase-3/7 by spectrofluorimetry **(C, D)**. WIF-B9 (**A, C, E**) and primary rat (**B, D, F**) healthy hepatocytes were treated or not (no EV) by 5 µg/mL EVs for 24 and 18 hours, respectively. EVs were isolated from WIF-B9 or primary rat parent hepatocytes exposed or not (CTRL-EV) to 100 nM BP (BP-EV), DBA (DBA-EV) or PYR (PYR-EV) for 72 hours and 18 hours, respectively. Some cultures were pre-treated for 30

minutes or not (-) with 6.25 mM thiourea (Th), a ROS scavenger, or 100 µM vitamin E (VitE), a free radical chain-breaking antioxidant. Values are given as means +/- standard deviation of 4 to 7 independent experiments. Treated with EVs *versus* untreated: ***p<0.001; Th, VitE pre-treated *versus* non pre-treated: #p<0.01.

Figure 7: Apoptosis of recipient hepatocytes is dependent on EV internalization by endocytosis and possibly on the pro-oxidant EV content, such as NADPH oxidase and iron. (**A**) Uptake of PKH-67-stained EVs by recipient WIF-B9 hepatocytes observed using confocal microscopy **(**left images**)** and quantified by spectrofluorimetry **(**right histogram**)**. **(B, C)** Apoptosis estimated by microscopic observation of the number of cells with condensed and/or fragmented chromatin after nuclear staining by Hoechst 33342. WIF-B9 (**A, C**) and primary rat (**C**) healthy hepatocytes were treated or not (no EV) by 5 µg/mL EVs for 24 and 18 hours, respectively. EVs were isolated from WIF-B9 or primary rat parent hepatocytes exposed or not (CTRL-EV) to 100 nM BP (BP-EV), DBA (DBA-EV) or PYR (PYR-EV) for 72 hours and 18 hours, respectively. Some cultures were pre-treated for 30 minutes or not (-) with 3 mM methyl-β-cyclodextrin (MCD), an inhibitor of lipid raft mediated endocytosis, 5 µg/mL cytochalasin B (CyB), 1 µM wortmannin (Wort), both inhibitors of endocytosis and phagocytosis, or 10 nM bafilomycin A (BAF), an inhibitor of lysosomal V-ATPase and hence lysosome activities. Some cultures were pre-treated for 30 minutes or not (-) with 300 µM apocynin (APO), an inhibitor of NADPH oxidase or 4 µM desferrioxamine (DFO), a lysosome specific LMW iron chelator, or 60 µM deferiprone (DFP), a LMW iron chelator in all cell compartments. Values are given as means ± standard deviation of 3 to 7 independent experiments. Treated with EVs *versus* untreated: *p<0.05 ; **p<0.01 ; ***p<0.001; CyB, Wort, BAF, APO, DFO, DFP pre-treated *versus* non pre-treated: #p<0.01.

Figure 8: EVs from PAH-treated parent hepatocytes alter lysosome morphology of recipient hepatocytes. (A, B) Confocal fluorescence microscopy after staining lysosomes of WIF-B9 (**A**) or primary rat (**B**) hepatocytes by the fluorescent probe LysoTracker. Punctuate red spots around the nucleus correspond to lysosomes with intact integrity. White arrows indicate lysosome permeabilization while solid white arrows show lysosome size increase. The images are representative of at least 4 independent experiments. (**C**) Transmission electron microscopy of WIF-B9 hepatocytes. Black and white arrows indicate lysosome size increase and lysosome membrane permeabilization, respectively. m: mitochondria l: lysosome n: nucleus. The images are representative of 2 independent experiments. WIF-B9 (**A, C**) and

primary rat (**B**) healthy hepatocytes were treated or not (no EV) by 5 µg/mL EVs for 24 and 18 hours, respectively. EVs were isolated from WIF-B9 or primary rat parent hepatocytes exposed or not (CTRL-EV) to 100 nM BP (BP-EV), DBA (DBA-EV) or PYR (PYR-EV) for 72 hours and 18 hours, respectively.

Figure 9: Mitochondrial free iron content. (**A**) Confocal fluorescence microscopy after staining mitochondria of WIFB9 hepatocytes by the fluorescent probes Mito-FerroGreen and MitoTracker red FM. Punctuate red spots correspond to mitochondria; green spots represent mitochondrial iron. (**B**) Mitochondrial iron content was quantified, cell by cell, by the relative ratio of green over red fluorescence. WIF-B9 hepatocytes were pre-treated for 30 minutes or not (-) with 4 µM desferrioxamine (DFO) and were exposed or not (no EV) to 5 µg/mL EVs for 24 hours. EVs were isolated from WIF-B9 parent hepatocytes exposed or not (CTRL-EV) to 100 nM BP (BP-EV). Treatment of cells to nitrilotriacetate iron (FeNTA) was used as a positive control for iron accumulation in mitochondria. The images are representative of 3 independent experiments. Treated with EVs or FeNTA *versus* no EVs : *$p<0.05$; **$p<0.01$, DFO pre-treated *versus* non pre-treated: #$p<0.05$.

Figure 10: Proposed mechanisms underlying the capacity of EVs derived from PAH-treated parent hepatocytes (PAH-EVs) to induce apoptosis in healthy recipient hepatocytes. PAH-EVs enriched in NADPH oxidase and ferritin are internalized in recipient hepatocytes, then trafficked towards lysosomes. In lysosomes, NADPH oxidase could be a source of superoxide anion that can be converted in H_2O_2; in parallel, hydrolases of lysosome lumen could degrade EV membrane and ferritin, thus providing LMW iron. H_2O_2 and iron can then promote the Fenton reaction leading to the highly oxidant free radical hydroxyl production and thus lipid peroxidation of lysosome membranes. The consecutive lysosomal membrane permeabilization could be upstream mitochondrion damages and apoptosis of recipient hepatocytes.

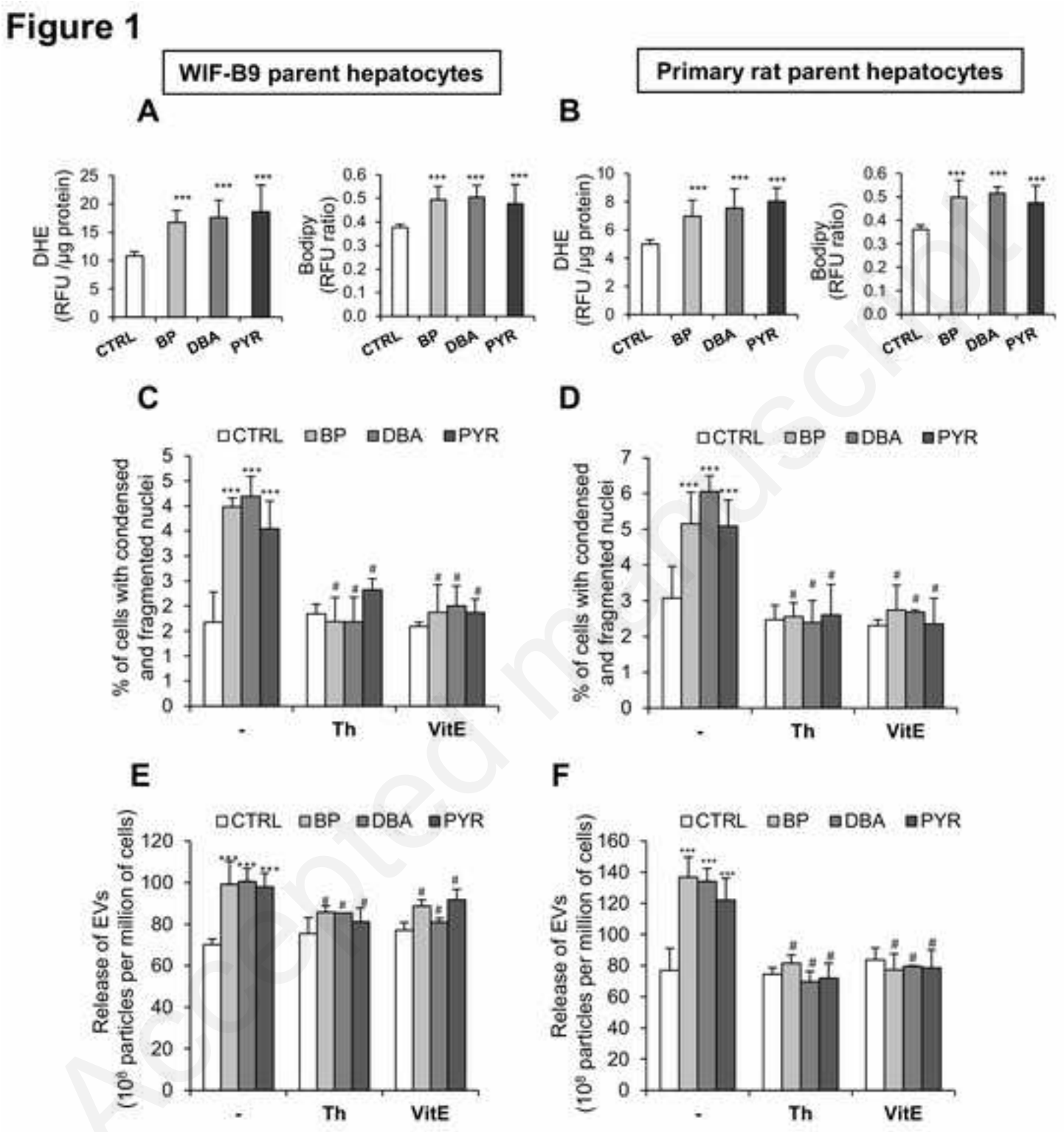

Figure 2

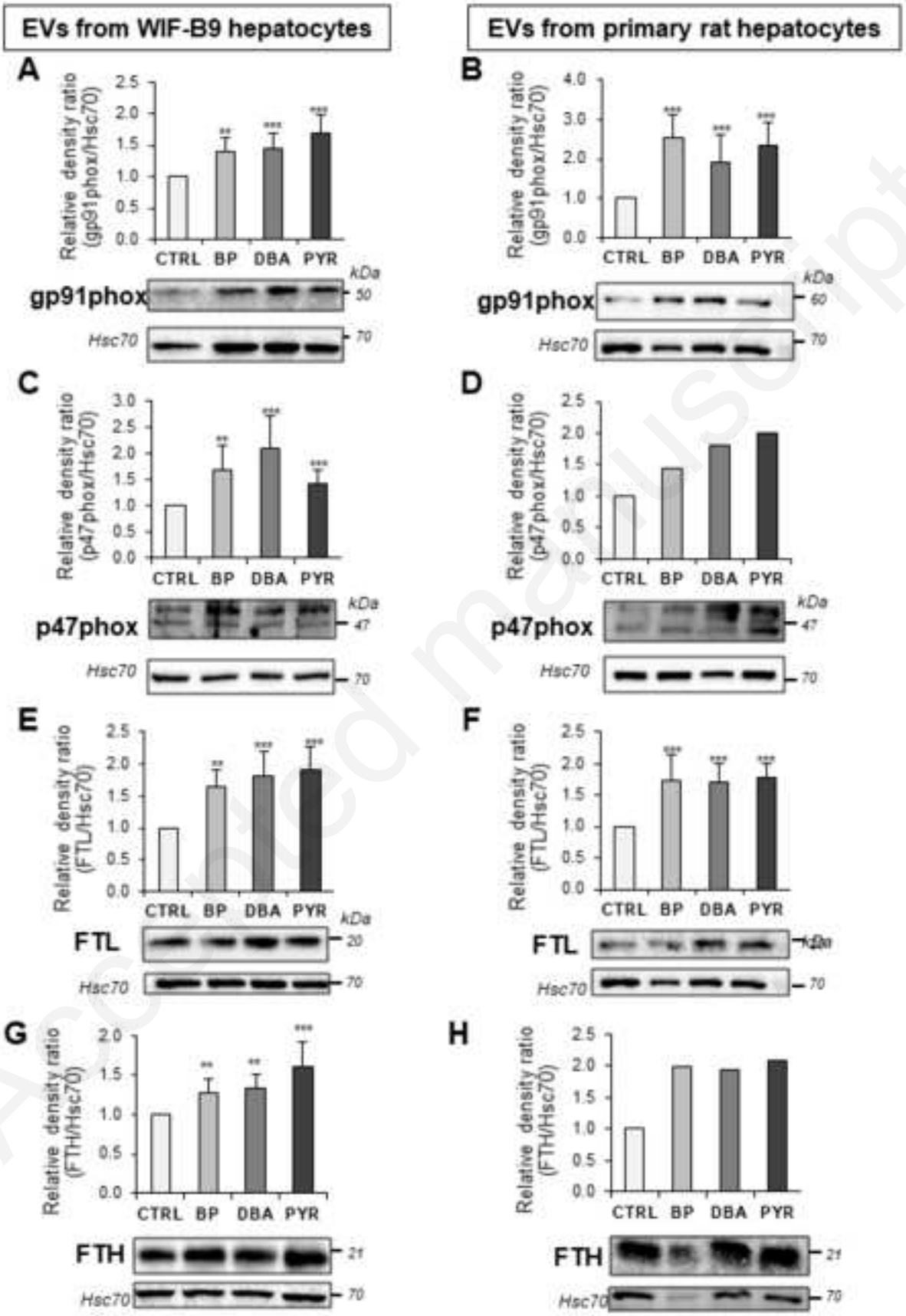

Figure 3

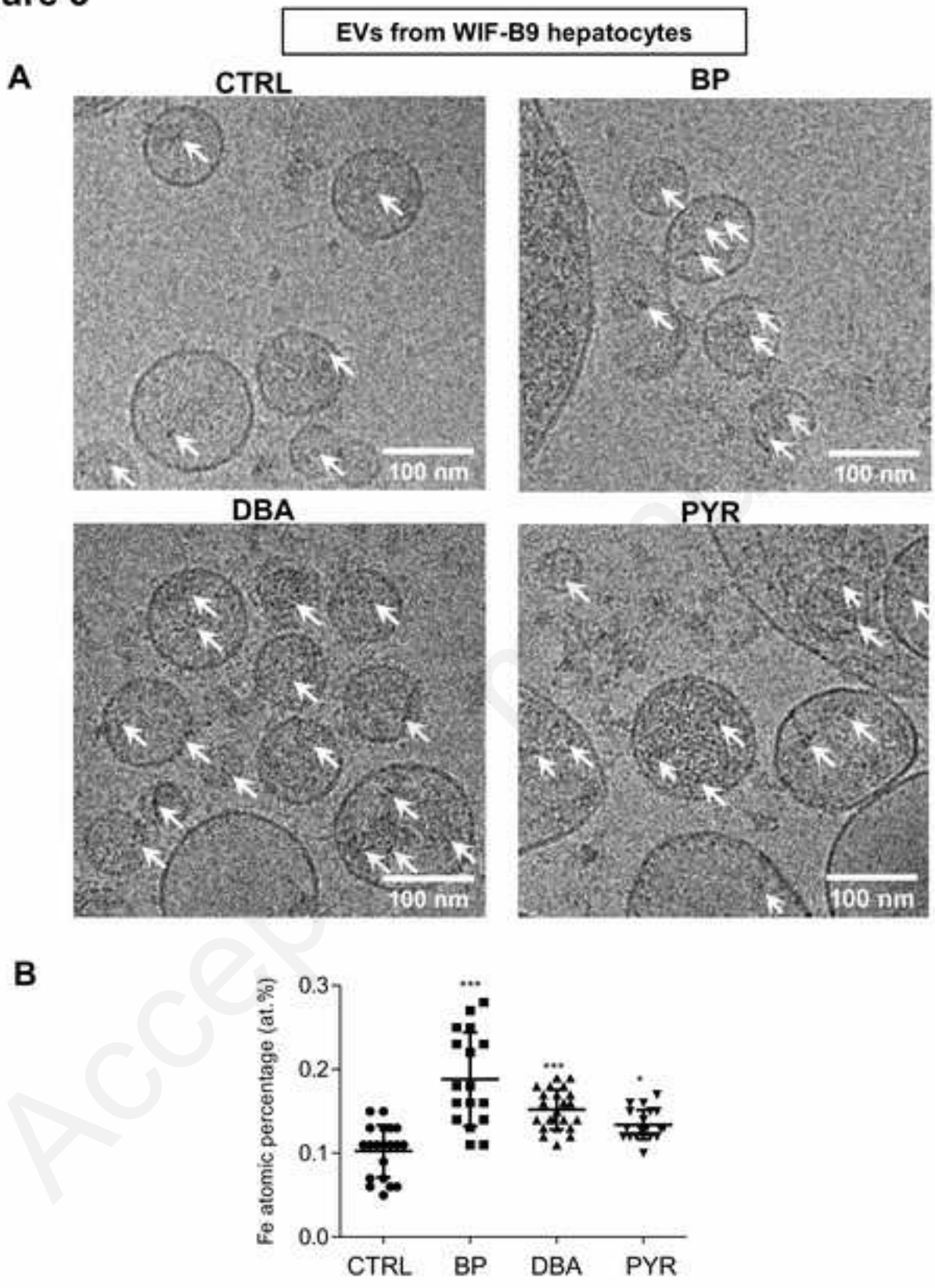
EVs from WIF-B9 hepatocytes
A
CTRL
BP
DBA
PYR
100 nm
100 nm
100 nm
100 nm
B
Fe atomic percentage (at.%)
0.3
0.2
0.1
0.0
CTRL
BP
DBA
PYR

Figure 4

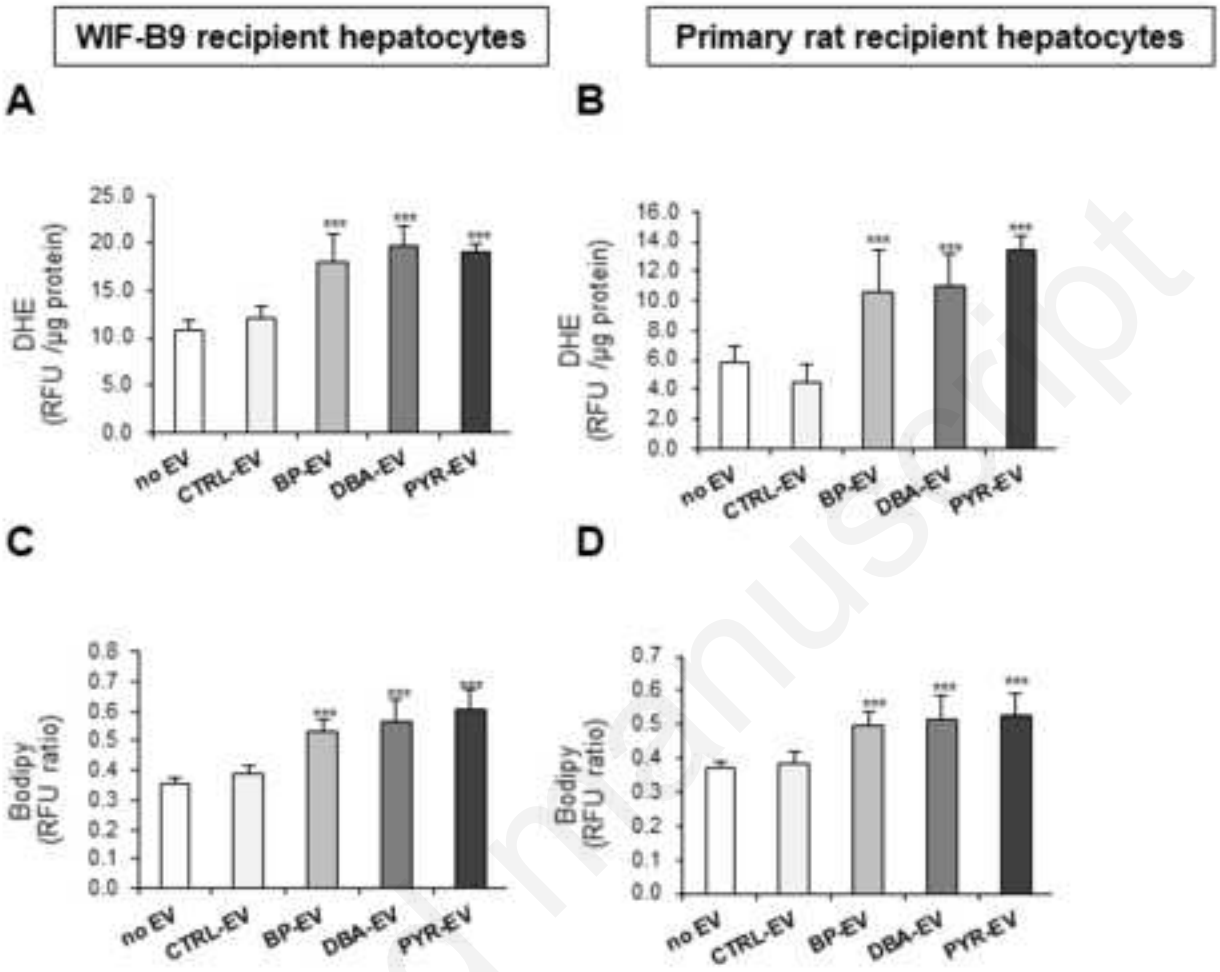

Figure 5A

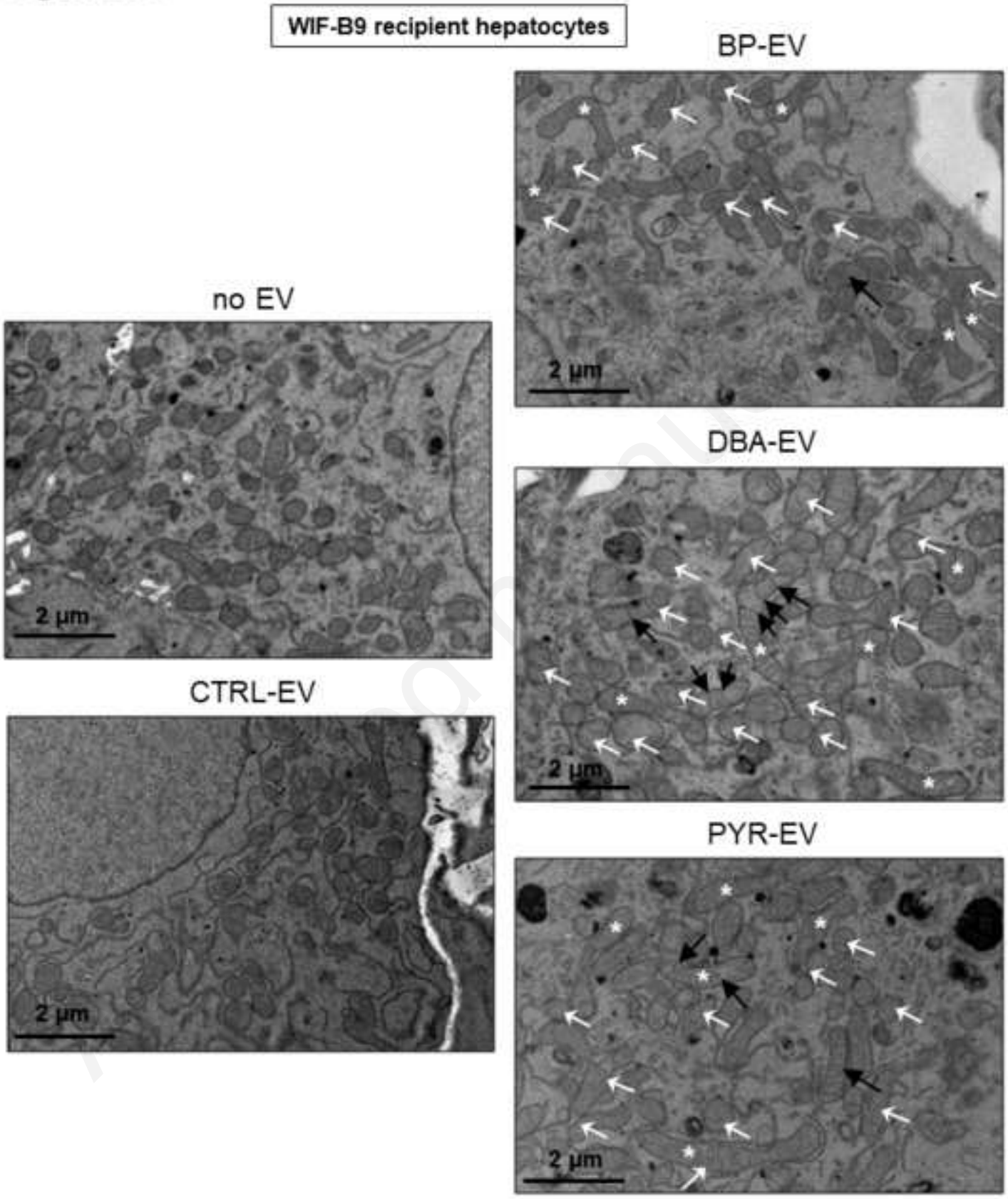

Figure 5B

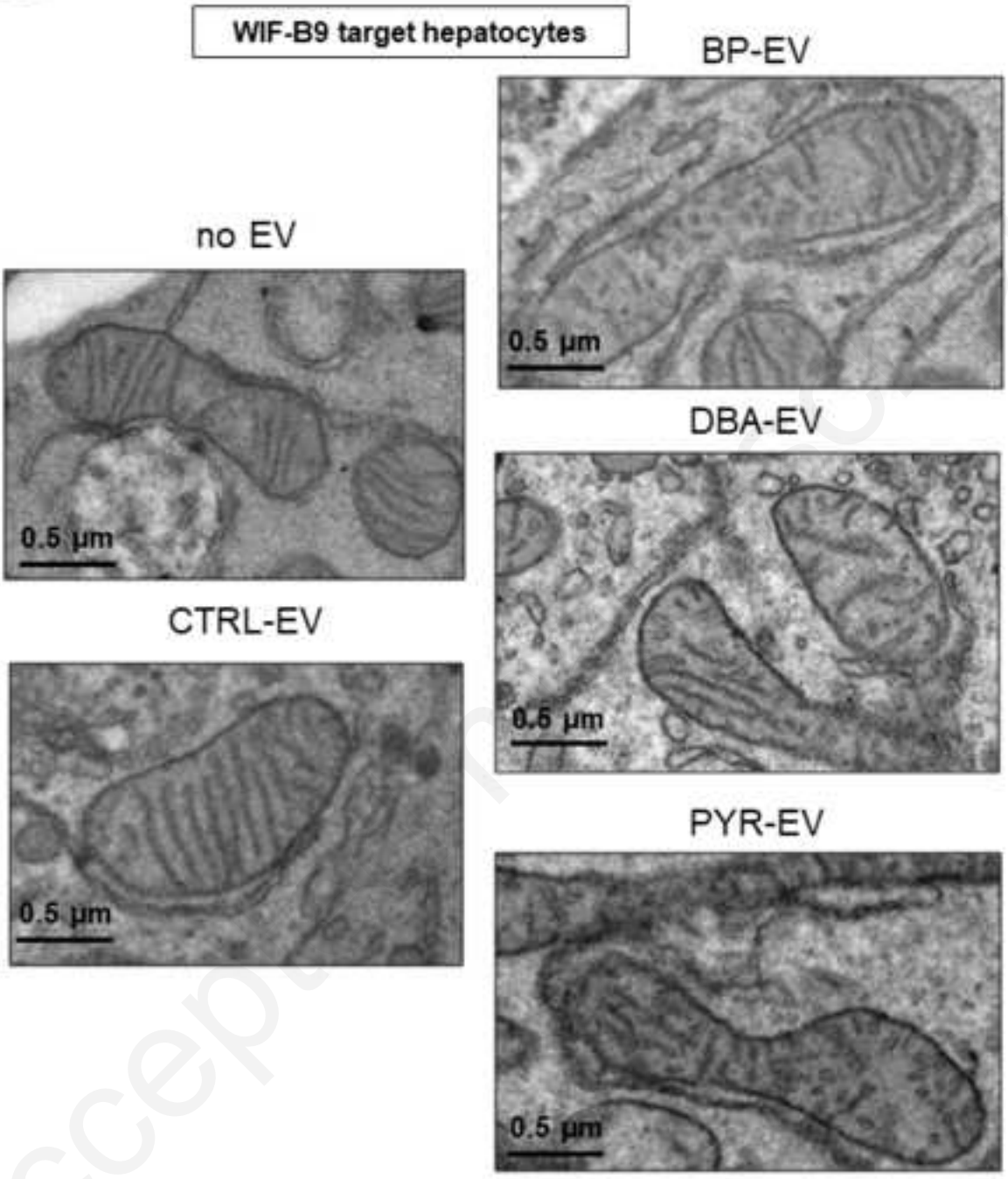

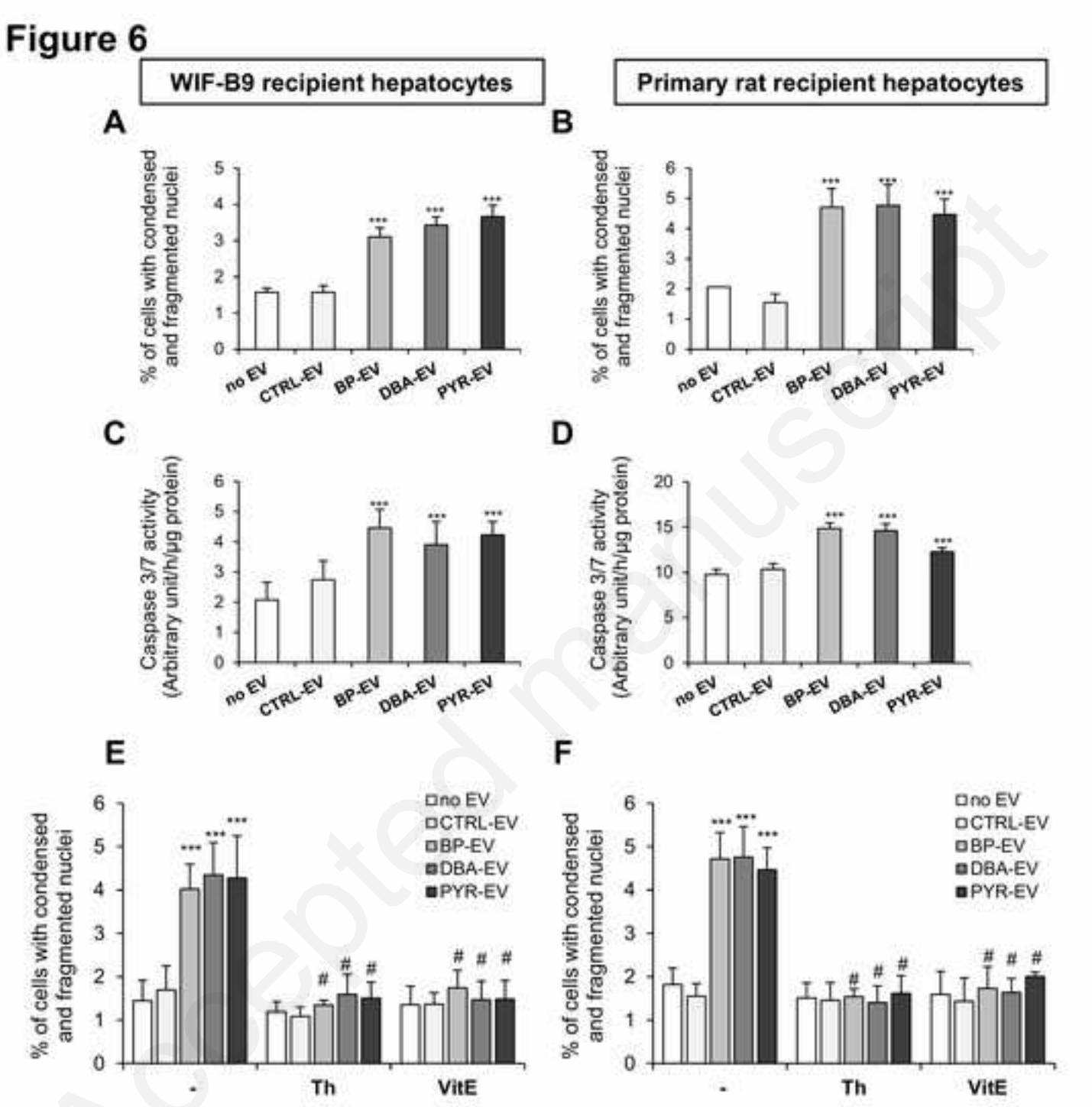

Figure 7

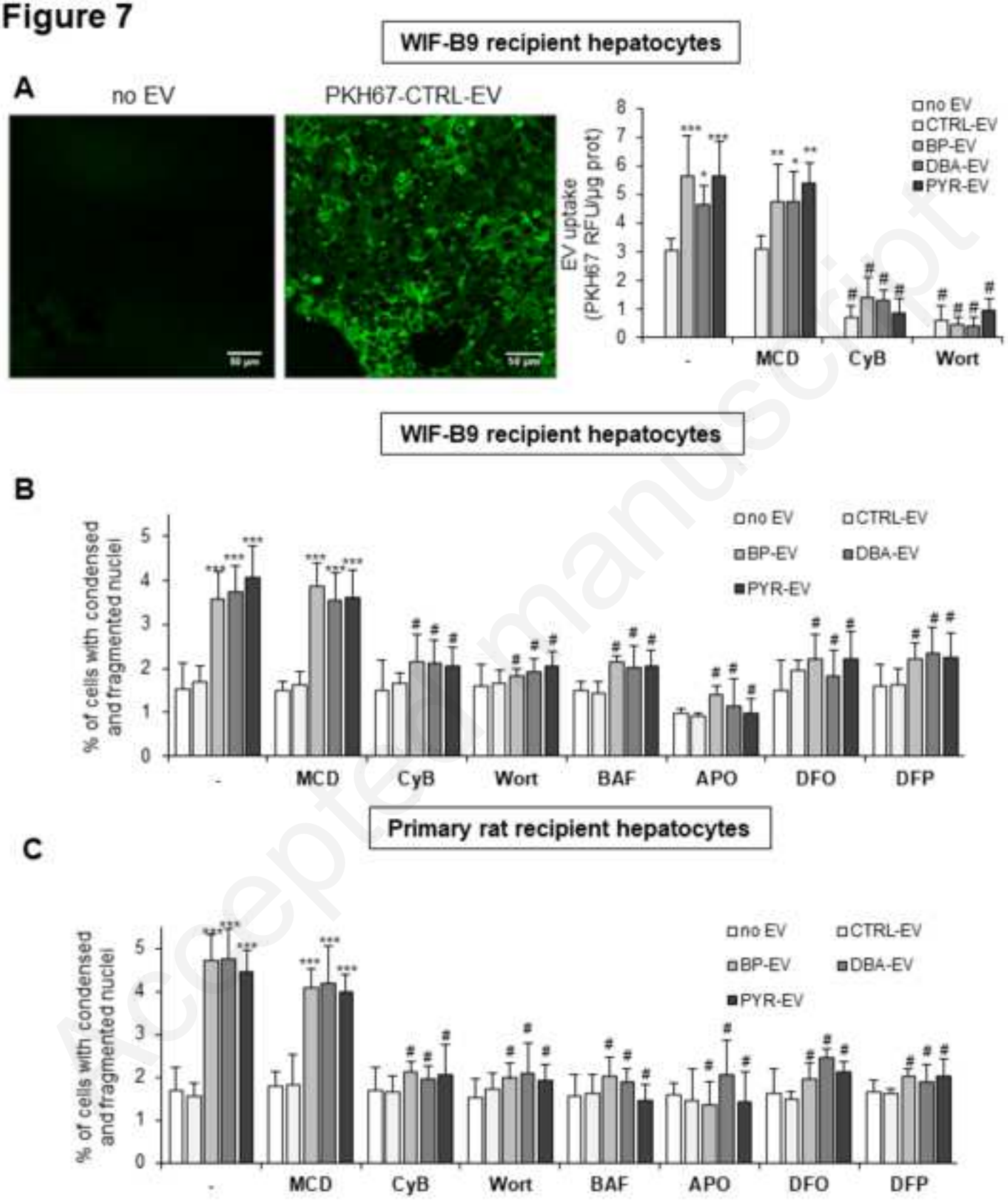

Figure 8

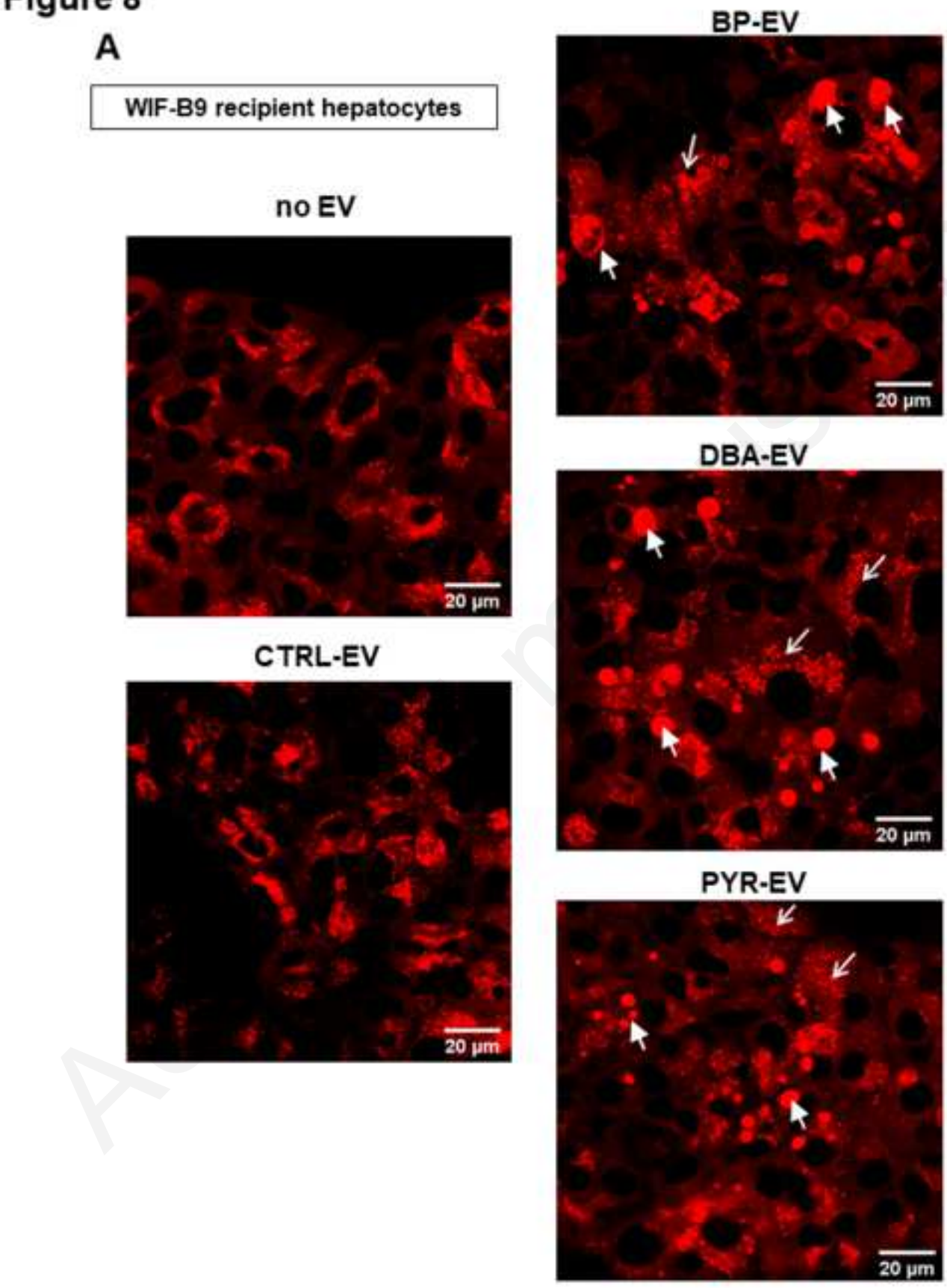

Figure 8
B

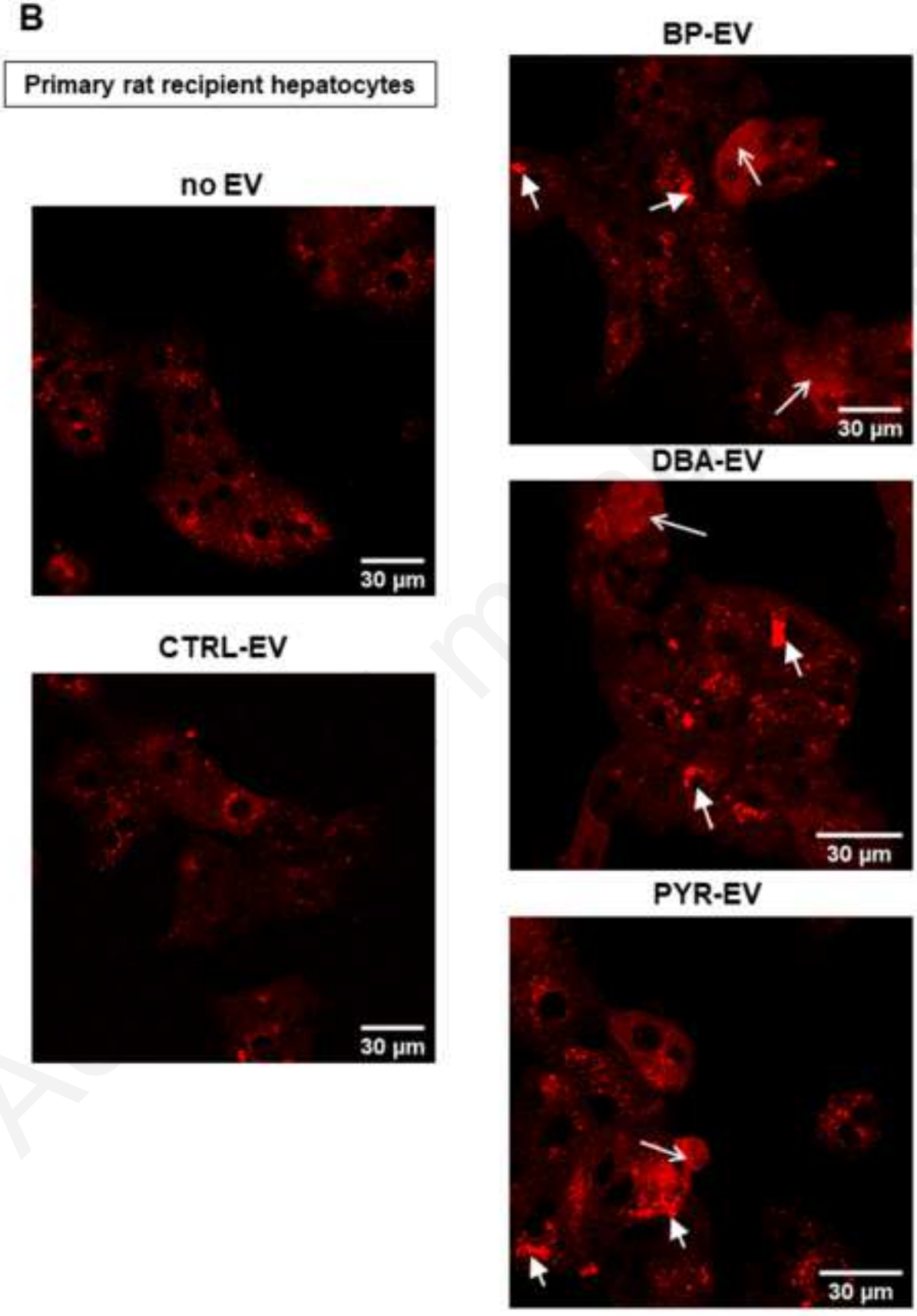

Figure 8
C

WIF-B9 recipient hepatocytes

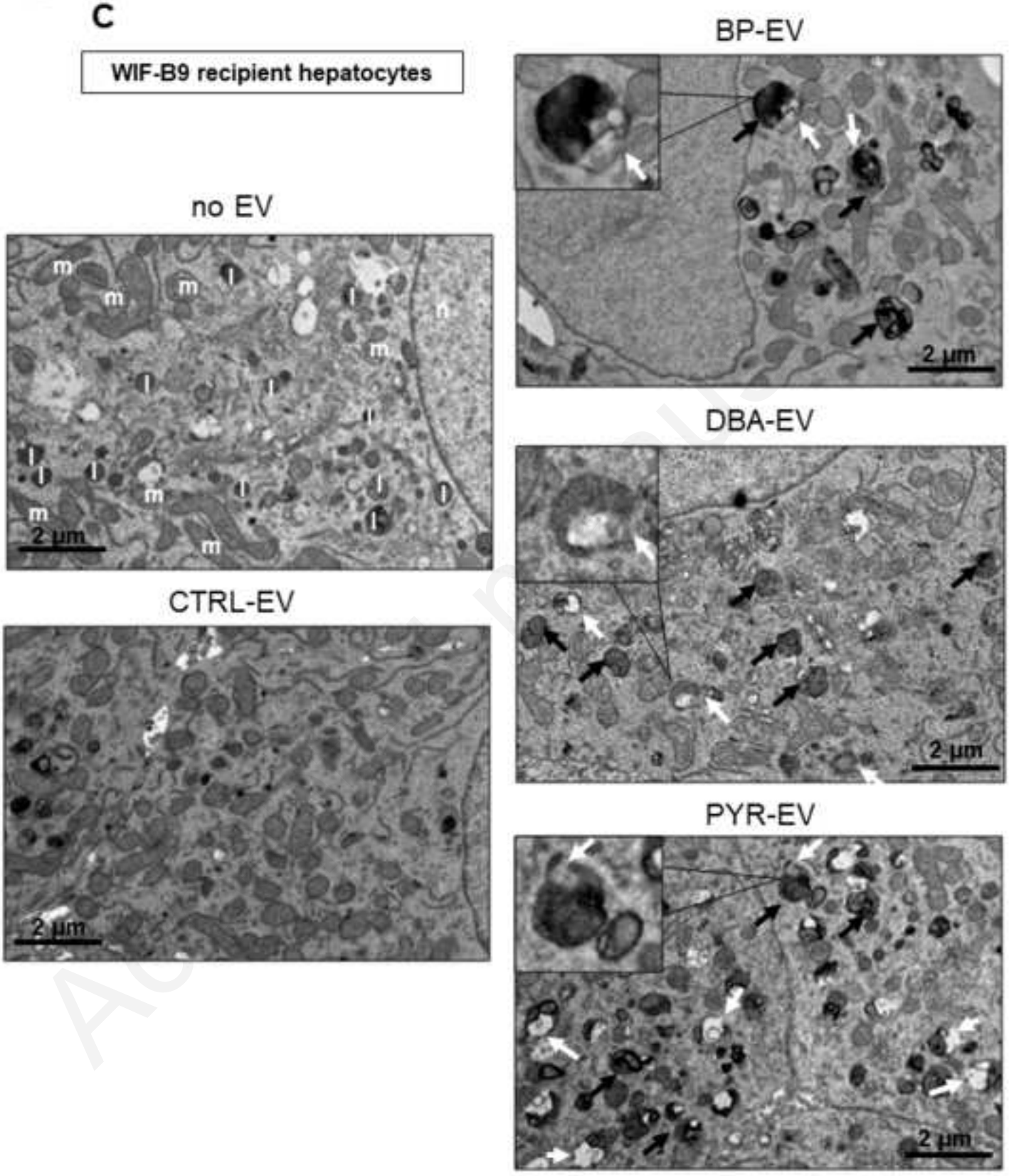

Figure 9

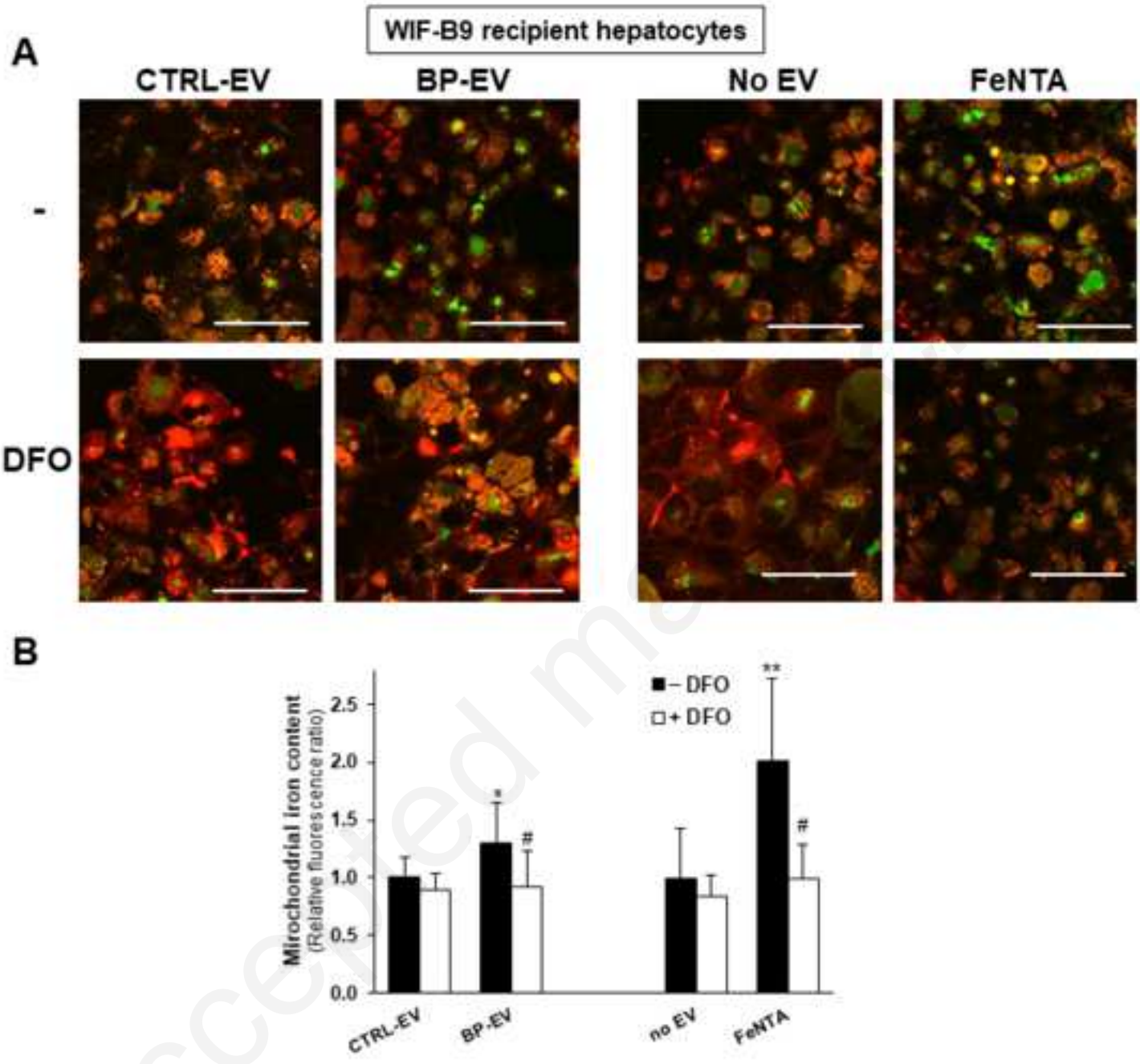

Figure 10